

1  
2  
3  
4  
5  
6  
7  
8  
9  
10  
11

# **Mass Accommodation and Gas-Particle Partitioning in Secondary Organic Aerosols: Dependence on Diffusivity, Volatility, Particle-phase Reactions, and Penetration Depth**

Manabu Shiraiwa<sup>1,\*</sup> and Ulrich Pöschl<sup>2,\*</sup>

1. Department of Chemistry, University of California, Irvine, CA92625, USA

2. Multiphase Chemistry Department, Max Planck Institute for Chemistry, 55128 Mainz, Germany

\* Correspondence to: [m.shiraiwa@uci.edu](mailto:m.shiraiwa@uci.edu); [u.poschl@mpic.de](mailto:u.poschl@mpic.de)

12 **Abstract.**

13 Mass accommodation is an essential process for gas-particle partitioning of organic compounds in  
14 secondary organic aerosols (SOA). The mass accommodation coefficient is commonly described  
15 as the probability of a gas molecule colliding with the surface to enter the particle phase. It is often  
16 applied, however, without specifying if and how deep a molecule has to penetrate beneath the  
17 surface to be regarded as incorporated into the condensed phase (adsorption vs. absorption). While  
18 this aspect is usually not critical for liquid particles with rapid surface-bulk exchange, it can be  
19 important for viscous semisolid or glassy solid particles to distinguish and resolve the kinetics of  
20 accommodation at the surface, transfer across the gas-particle interface, and further transport into  
21 the particle bulk.

22 For this purpose, we introduce a novel parameter: an effective mass accommodation coefficient  
23  $\alpha_{\text{eff}}$  that depends on penetration depth and is a function of surface accommodation coefficient,  
24 volatility, bulk diffusivity, and particle-phase reaction rate coefficient. Application of  $\alpha_{\text{eff}}$  in the  
25 traditional Fuchs-Sutugin approximation of mass-transport kinetics at the gas-particle interface  
26 yields SOA partitioning results that are consistent with a detailed kinetic multilayer model (KM-  
27 GAP, Shiraiwa et al. 2012) and two-film model solutions (MOSAIC, Zaveri et al., 2014) but  
28 deviate substantially from earlier modeling approaches not considering the influence of penetration  
29 depth and related parameters.

30 For highly viscous or semisolid particles, we show that the effective mass accommodation  
31 coefficient remains similar to the surface accommodation coefficient in case of low-volatile  
32 compounds, whereas it can decrease by several orders of magnitude in case of semi-volatile  
33 compounds. Such effects can explain apparent inconsistencies between earlier studies deriving  
34 mass accommodation coefficients from experimental data or from molecular dynamics  
35 simulations.

36 Our findings challenge the approach of traditional SOA models using the Fuchs-Sutugin  
37 approximation of mass transfer kinetics with a fixed mass accommodation coefficient regardless  
38 of particle phase state and penetration depth. The effective mass accommodation coefficient  
39 introduced in this study provides an efficient new way of accounting for the influence of volatility,  
40 diffusivity, and particle-phase reactions on SOA partitioning in process models as well as in  
41 regional and global air quality models. *While kinetic limitations may not be critical for partitioning  
42 into liquid SOA particles in the planetary boundary layer (PBL), the effects are likely important*

43 for amorphous semi-solid or glassy SOA in the free and upper troposphere (FT/UT) as well as in  
44 the PBL at low relative humidity and low temperature.

45

## 46 **1. Introduction.**

47 Secondary organic aerosols (SOA) are major constituents of atmospheric particulate  
48 matter, affecting air quality, climate, and public health (Jimenez et al., 2009; Kanakidou et al.,  
49 2005; Pöschl and Shiraiwa, 2015; Shrivastava et al., 2017a). Gas-phase reactions of volatile  
50 organic compounds (VOC) emitted from various anthropogenic and biogenic sources with  
51 oxidants such as ozone and OH radicals lead to the formation and growth of SOA (Kroll and  
52 Seinfeld, 2008). The oxidation of VOC forms a myriad of semi-volatile (SVOC) and low volatility  
53 organic compounds (LVOC) that can condense on pre-existing particles (Ziemann and Atkinson,  
54 2012) or contribute to nucleation and new particle formation (Tröstl et al., 2016). The evolution of  
55 SOA is a complex multi-step process that involves chemical reactions and mass transport in the gas  
56 phase, at the particle surface and in the particle bulk, but the interplay of these processes and the  
57 rate-limiting steps in SOA formation have not yet been fully resolved/elucidated (Shiraiwa et al.,  
58 2014).

59 Traditionally, SOA particles were assumed to be homogeneous and well-mixed quasi-  
60 liquid droplets (Pankow, 1994). As demonstrated by recent atmospheric measurements and  
61 laboratory experiments, they can adopt glassy solid or amorphous semi-solid phase states,  
62 challenging the traditional views of SOA properties, interactions and effects (Koop et al., 2011;  
63 Reid et al., 2018; Virtanen et al., 2010). Slow diffusion of water, oxidants and organic molecules  
64 in viscous, semi-solid, or glassy particles may lead to kinetic limitations in heterogeneous and  
65 multiphase reactions (Alpert et al., 2019; Davies and Wilson, 2015; Kuwata and Martin, 2012;  
66 Shiraiwa et al., 2011; Zhang et al., 2018; Zhou et al., 2019). Global model calculations suggest  
67 that the phase state of atmospheric SOA may vary between liquid, semi-solid and solid in the  
68 planetary boundary layer, while SOA should be mostly in a glassy state in the free troposphere  
69 (Shiraiwa et al., 2017). The occurrence of glassy SOA in the free troposphere may promote ice  
70 nucleation and cloud droplet activation (Knopf et al., 2018; Slade et al., 2017) and facilitate long-  
71 range transport of toxic organic compounds contained in SOA (Mu et al., 2018; Shrivastava et al.,  
72 2017b).

73 The formation and properties of SOA are large sources of uncertainty in the current  
74 understanding of global air quality, climate change, and public health. The development of SOA  
75 models is among the most challenging problems in atmospheric chemistry (Tsigaridis et al., 2014).  
76 In most current air quality, atmospheric chemistry and climate models, the limiting step of SOA

77 formation is assumed to be gas-phase oxidation of VOC to form semi-volatile and low volatile  
78 products. Thus, gas-phase oxidation is described kinetically, while gas-particle partitioning is often  
79 approximated by quasi-instantaneous equilibrium partitioning of the oxidation products (Pankow,  
80 1994; Shrivastava et al., 2017a; Tsigaridis et al., 2014). The assumption of quasi-instantaneous  
81 gas-particle equilibration, however, is in question if particles are highly viscous, semi-solid or  
82 glassy - especially at low temperatures and low relative humidity (RH) (Li and Shiraiwa, 2019;  
83 Shiraiwa and Seinfeld, 2012). Experimental studies found kinetic limitations for gas uptake and  
84 particle evaporation at low RH (Liu et al., 2016; Perraud et al., 2012; Vaden et al., 2011; Yli-Juuti  
85 et al., 2017), but not for mixing in SOA at medium or high RH (Ye et al., 2016; Ye et al., 2018).  
86 An appropriate treatment of kinetic limitations depending on ambient conditions is critical for  
87 accurately reproducing particle size distribution dynamics in SOA growth (Shiraiwa et al., 2013a;  
88 Zaveri et al., 2018; Zaveri et al., 2020).

89 The dynamics of gas-particle partitioning have been considered in a wide range of  
90 atmospheric aerosol models, including aerosol dynamics models (Liu et al., 2019; McVay et al.,  
91 2014; Pandis et al., 1993; Riipinen et al., 2011; Zaveri et al., 2014), kinetic multilayer models  
92 (Berkemeier et al., 2016; Fowler et al., 2018; Roldin et al., 2014; Shiraiwa et al., 2012), GECKO-  
93 A (Aumont et al., 2005), the volatility basis set approach (Trump and Donahue, 2014; Trump et  
94 al., 2014), the statistical oxidation model (Cappa et al., 2016; Jathar et al., 2016), and particle  
95 evaporation models (Vaden et al., 2011; Yli-Juuti et al., 2017). Most model studies are using the  
96 Fuchs-Sutugin approximation of mass-transport kinetics at the gas-particle interface with a fixed  
97 mass accommodation coefficient that does not vary with particle phase state nor with the volatility  
98 and diffusivity of the investigated organic compounds. Molecular dynamics simulations (Julin et  
99 al., 2014; Von Domaros et al., 2020) and a recent SOA chamber study (Liu et al., 2019) suggest  
100 that the mass accommodation coefficients for semi-volatile organic molecules on organic  
101 substrates are close to unity. Measurement-derived mass accommodation coefficients reported  
102 from thermodenuder investigations of SOA volatility distributions, however, were one to three  
103 orders of magnitude lower (Kostenidou et al., 2018; Lee et al., 2010; Saleh et al., 2011).

104 Overall, the relations between particle phase state, mass accommodation, and the growth  
105 and atmospheric evolution of SOA have not yet been resolved and continue to be a subject of  
106 scientific debate. In this study, we investigate the influence of volatility, diffusivity, and particle  
107 phase state on the mass accommodation and gas-particle partitioning of organic compounds in

108 SOA by detailed and simplified kinetic modeling approaches, comparing the Fuchs-Sutugin  
109 approximation to a detailed kinetic multilayer model (KM-GAP, Shiraiwa et al. 2012) as well as  
110 approximate and transient two-film model solutions (MOSAIC, Zaveri et al., 2014).

111

## 112 2. Theory and Methods

113 Traditionally, dynamic models of aerosol chemistry and physics describe the rate of gas-  
114 particle partitioning by a first-order gas-particle mass transfer coefficient ( $k_{gp}$  in  $s^{-1}$ ) based on the  
115 Fuchs-Sutugin approximation of gas diffusion in the transition regime (Seinfeld and Pandis, 2016):

$$116 \quad k_{gp} = 4 \pi D_g r_p N_p \beta \quad (1)$$

$$117 \quad \beta = \frac{0.75 \alpha (1+Kn)}{Kn^2+Kn+0.283 Kn \alpha+0.75\alpha} \quad (2)$$

118 where  $D_g$  ( $cm^2 s^{-1}$ ) is the gas phase diffusivity,  $r_p$  (cm) is the particle radius,  $N_p$  ( $cm^{-3}$ ) is the particle  
119 number concentration,  $Kn$  is the Knudsen number, and  $\alpha$  is the mass accommodation coefficient  
120 which represents the probability for a gas molecule colliding with the surface of the particles to  
121 enter the condensed phase.  $k_{gp}$  is also often termed as condensation sink (CS).  $Kn$  is the ratio of  
122 the mean free path in the gas phase ( $\lambda$ ), which can be calculated using the mean thermal velocity  
123 ( $\omega$ ), and the particle radius:  $Kn = \lambda / r_p = 3 D_g / (\omega r_p)$  (Pöschl et al., 2007). The Fuchs-Sutugin  
124 correction is validated by experiments with  $\sim 6 \times 10^{-3} < Kn < 10$  (Seinfeld & Pandis, 2016). With a  
125 typical mean free path of  $\sim 100$  nm for SOA compounds, this range corresponds to  $10 \text{ nm} < r_p <$   
126  $\sim 17 \text{ }\mu\text{m}$ , covering a typical size range of SOA particles observed in ambient atmosphere and  
127 laboratory experiments.  $\beta$  is the transition regime correction factor, which depends on  $Kn$  and  $\alpha$ .  
128 This approach was demonstrated to work well for simulating the hygroscopic growth of sub-10  
129 nm particles into few micron-size droplets, covering the kinetic and transition regimes (Winkler et  
130 al., 2006; Winkler et al., 2004). Note that for larger particles with the limit of  $Kn \rightarrow 0$ ,  $\beta$  approaches  
131 1 and the effect of mass accommodation coefficient becomes negligibly small in the continuum  
132 regime.

133 According to the absorptive partitioning theory under the assumption of ideal mixing  
134 (Pankow, 1994; Trump and Donahue, 2014), the rate of change of the gas- and particle-phase mass  
135 concentrations ( $C^g$ ,  $C^p$ ) of an organic compound in SOA partitioning can be expressed as:

$$136 \quad \frac{dC^g}{dt} = -k_{gp} \left( C^g - \frac{C^g}{C_{OA}} C^0 \right) \quad (3)$$

137 
$$\frac{dC^P}{dt} = k_{gp} \left( C^g - \frac{C^P}{C_{OA}} C^0 \right) - k_b C^P \quad (4)$$

138 where  $C_{OA}$  ( $\mu\text{g m}^{-3}$ ) is the organic aerosol particle mass concentration,  $C^0$  ( $\mu\text{g m}^{-3}$ ) is the gas phase  
 139 saturation mass concentration of the pure organic compound, and  $k_b$  ( $\text{s}^{-1}$ ) is the first-order rate  
 140 coefficient for its reaction in the particle bulk. The term  $\frac{C^P}{C_{OA}} C^0$  represents gas-phase concentration  
 141 of Z right at the surface and condensation is driven by gas-phase concentration gradient of Z  
 142 between the gas and condensed phases.

143 While the term mass accommodation coefficient is widely used in atmospheric aerosol  
 144 studies, its precise meaning is not always well defined. In particular,  $\alpha$  is often applied without  
 145 specifying if and how deep a molecule has to penetrate beneath the surface to have entered the  
 146 condensed phase (adsorption vs. absorption). This aspect is usually not critical for liquid droplets  
 147 with rapid surface-bulk exchange, fast bulk diffusion, and swift equilibration between the  
 148 condensed phase and the surrounding gas phase. For viscous or solid particles, however, it can be  
 149 essential to distinguish and resolve the kinetics of surface and bulk processes, including  
 150 accommodation at the surface, transfer across the gas-particle interface, and further transport into  
 151 the particle bulk (Kolb et al., 2010; Pöschl et al., 2007; Shiraiwa et al., 2012).

152 Building on the PRA kinetic model framework (Pöschl et al., 2007) and the kinetic  
 153 multilayer model of surface chemistry and gas-particle interactions in aerosols and clouds (KM-  
 154 GAP; Shiraiwa et al., 2012), we have derived an expression for the mass accommodation  
 155 coefficient as a function of penetration depth into the particle bulk and related parameters (see  
 156 step-by-step derivation in Appendix):

157 
$$\alpha(x) = \alpha_s \frac{1}{1 + \frac{\alpha_s \omega C^0}{4 D_b \rho_p} x \cdot 10^{-12} \frac{\text{g cm}^{-3}}{\mu\text{g m}^{-3}}} \quad (5)$$

158 Here  $\omega$  ( $\text{cm s}^{-1}$ ) is the mean thermal velocity of the organic compound in the gas phase,  $D_b$   
 159 ( $\text{cm}^2 \text{s}^{-1}$ ) is its diffusivity in the condensed phase,  $\rho_p$  ( $\text{g cm}^{-3}$ ) is the particle density, and  $x$  (cm) is  
 160 the penetration depth. The scaling factor  $10^{-12} (\text{g cm}^{-3})/(\mu\text{g m}^{-3})$  allows for inserting  $C^0$  in the  
 161 commonly used units of  $\mu\text{g m}^{-3}$ ; it can be omitted when  $C^0$  is inserted in  $\text{g cm}^{-3}$  or when all  
 162 quantities are inserted with standard SI units (cgs or mks system of units).

163 The surface accommodation coefficient  $\alpha_s$ , which corresponds to  $\alpha(0)$  with the penetration  
 164 depth of 0, is the probability for a gas molecule Z colliding with the surface not to be immediately

165 scattered back to the gas phase but to be accommodated at the surface for period longer than the  
 166 duration of an elastic scattering process (Pöschl et al., 2007). Various equivalent, similar or closely  
 167 related terms and parameters have been defined and used in the scientific literature include (Kolb  
 168 et al., 2010; Pöschl et al., 2007): the condensation coefficient (Pruppacher and Klett, 1997),  
 169 adsorption coefficient (Shi et al., 1999; Turco et al., 1989; Worsnop et al., 2002), sticking  
 170 coefficient (Hanson, 1997), sticking probability (Clement et al., 1996; Garrett et al., 2006),  
 171 trapping probability (Masel, 1996), adsorptive mass accommodation coefficient (Elliott et al.,  
 172 1991), and thermal accommodation coefficient (Li et al., 2001; Worsnop et al., 2002).

173 When the penetration depth equals one or two molecular layers, i.e., once or twice the  
 174 effective molecular length or diameter ( $\delta$ ), the corresponding penetration-depth-dependent mass  
 175 accommodation coefficient is equivalent to the quasi-static surface accommodation coefficient  
 176 ( $\alpha_{ss}$ ) or bulk accommodation coefficient ( $\alpha_b$ ), respectively, as defined in earlier kinetic multilayer  
 177 model studies (Shiraiwa et al., 2012):  $\alpha(\delta) = \alpha_{ss}$  and  $\alpha(2\delta) = \alpha_b$ . A recent study has compared this  
 178 kinetic multilayer (KM) modeling approach with molecular dynamics (MD) simulations to  
 179 calculate mass accommodation coefficients for a variety of semi-volatile compounds with different  
 180 volatilities in squalene (Von Domaros et al., 2020). The penetration depth was assumed to be equal  
 181 to the sum of half of the molecule's own length and half of the length of a squalene molecule. For  
 182 the evaluation of uncertainties and sensitivities, the penetration depth was also varied from semi-  
 183 volatile molecule's own length as a lower bound to the half-width of the nonuniform free energy  
 184 region determined by the MD free energy profile as an upper bound. Within this range, the results  
 185 of MD and KM simulations were in good agreement with each other, confirming the consistency  
 186 and validity of the multilayer approach (Von Domaros et al., 2020).

187 Using the two-film theory of mass transfer between gas and particle phases, Zaveri et al.  
 188 (2014) showed that the effects of a concentration gradient in the particle can be represented by a  
 189 thin film adjacent to the surface with the following thickness or effective penetration depth for  
 190 non-reactive partitioning and reactive uptake, respectively:

$$191 \quad x_{\text{eff}} = r_p / 5 \quad (\text{non-reactive partitioning}) \quad (6)$$

$$192 \quad x_{\text{eff}} = r_p \left( \frac{1-Q}{q \coth q - 1} \right) \quad (\text{reactive uptake}) \quad (7)$$

193 where  $Q$  is the ratio of the average particle-phase concentration to the surface concentration at  
 194 steady state and  $q$  is a dimensionless diffusion-reaction parameter (Seinfeld and Pandis, 2016):



195 
$$Q = 3 \left( \frac{q \coth q - 1}{q^2} \right) \quad (8)$$

196 
$$q = r_p \sqrt{\frac{k_b}{D_b}} \quad (9)$$

197 Note that  $q$  is the ratio of the particle radius to the so-called reacto-diffusive length,  $(D_b/k_b)^{0.5}$ ,  
 198 representing the characteristic depth to which a species can penetrate while reacting in the particle  
 199 bulk (Pöschl et al., 2007; Worsnop et al., 2002). The effective penetration depth represents the  
 200 depth from the surface where concentration gradients are confined under a quasi-steady state  
 201 (Zaveri et al., 2014). The timescale for molecules to travel effective penetration depth ( $\tau_{x_{\text{eff}}}$ ) can  
 202 be estimated by the Fick's law:  $\tau_{x_{\text{eff}}} = x_{\text{eff}}^2 / D_b$ .

203 By inserting  $x_{\text{eff}}$  in equation (5), we obtain an effective mass accommodation coefficient  
 204 that accounts for the influence of penetration depth and its dependence on the diffusivity and  
 205 reactivity of the investigated chemical species in the particle:

206 
$$\alpha_{\text{eff}} = \alpha(x_{\text{eff}}) \quad (10)$$

207  $\alpha_{\text{eff}}$  can be combined into the transition regime correction factor ( $\alpha = \alpha_{\text{eff}}$  in Eq. 2) to account for  
 208 effective penetration depth in the Fuchs-Sutugin approach. This method should work after the  
 209 effective penetration depth is established under quasi-steady-state conditions, while the method  
 210 may underestimate condensation in transient conditions at shorter timescales as detailed below.  
 211 Following up on the helpful comments of an anonymous reviewer (Referee, 2020), we would like  
 212 to clarify that we consider the surface accommodation coefficient as a fundamental kinetic  
 213 parameter as defined by the PRA framework (Pöschl et al., 2007) – regardless of the specific mass  
 214 transfer regime – and not just as a parameter defined by Eq. 2. The effective accommodation  
 215 coefficient, on the other hand, comprises both the fundamental quantity  $\alpha_s$  and a flux correction  
 216 depending on the effective penetration depth as defined by Eqs. (5)-(10).

217

### 218 3. Results and Discussion

219 To investigate and demonstrate the relevance of the kinetics of mass accommodation and  
 220 the applicability of  $\alpha_{\text{eff}}$ , we simulate the temporal evolution of partitioning and equilibration of  
 221 semi-volatile organic compounds (SVOC) with  $C^0 = 100 \mu\text{g m}^{-3}$  and  $D_g = 0.1 \text{ cm}^2 \text{ s}^{-1}$  interacting  
 222 with non-volatile seed particles with a number concentration of  $5000 \text{ cm}^{-3}$ , an initial diameter of

223 200 nm, and a surface accommodation coefficient  $\alpha_s = \alpha(0) = 1$ . For the SVOC, we assume initial  
 224 gas- and particle-phase concentrations of  $2 \mu\text{g m}^{-3}$  and  $0 \mu\text{g m}^{-3}$ , respectively. The particles are  
 225 assumed to be either liquid with a bulk diffusion coefficient  $D_b = 10^{-7} \text{ cm}^2 \text{ s}^{-1}$  or semisolid with  $D_b$   
 226  $= 10^{-15} \text{ cm}^2 \text{ s}^{-1}$ . These conditions were adopted from model simulations by Zaveri et al. (2014),  
 227 representing typical conditions for SOA formation in laboratory experiments and ambient  
 228 atmosphere.

229 Model calculations were performed with the detailed kinetic multilayer model of gas-  
 230 particle interactions (KM-GAP, Shiraiwa et al. 2012), with the Model for Simulating Aerosol  
 231 Interactions and Chemistry (MOSAIC; Zaveri et al., 2014), and with an aerosol dynamic model  
 232 using the simple Fuchs-Sutugin gas-phase diffusion model (F-S) with different values of  $\alpha_m$ . Here,  
 233 the KM-GAP results can be regarded as a benchmark, because the KM-GAP model explicitly  
 234 resolves all relevant processes - including gas diffusion, reversible adsorption, surface-bulk  
 235 exchange, bulk diffusion, and condensed-phase reactions - and has been successfully validated by  
 236 against experimental data of both non-reactive partitioning and reactive gas uptake in a wide range  
 237 of aerosol and surrogate systems (Berkemeier et al., 2017; Shiraiwa et al., 2012). The MOSAIC  
 238 model yields approximate and transient solutions building on a less detailed representation of gas-  
 239 particle interactions, which does not resolve reversible adsorption and surface-bulk exchange  
 240 (Zaveri et al., 2014). In the F-S approximation, the kinetics of particle-phase mass transport are  
 241 represented only by  $\alpha_m$  as inserted into Eq. (2).

242 For liquid particles with fast surface-bulk exchange and bulk diffusion ( $D_b = 10^{-7} \text{ cm}^2 \text{ s}^{-1}$ ),  
 243  $\alpha(x)$  remains close to  $\alpha_s = \alpha(0) = 1$ , and all models yield the same result of fast mass transfer from  
 244 the gas to particle phase and equilibration within one second (all model lines overlap with the blue  
 245 dashed line (F-S,  $\alpha = 1$ ) in Fig. 1a). For semi-solid particles with  $D_b = 10^{-15} \text{ cm}^2 \text{ s}^{-1}$ , however, the  
 246 temporal evolution of the SVOC gas-phase and particle-phase concentrations varies between  
 247 different models and different values of  $\alpha$  as shown in Figure 1 on logarithmic scales.

248 According to KM-GAP (black line), the initial uptake of SVOC by the semisolid particle  
 249 phase is as fast as approximated by F-S with  $\alpha = \alpha_{ss} = \alpha_z(\delta) = 3 \times 10^{-2}$  corresponding to a  
 250 penetration depth of only one molecular length (monolayer) below the particle surface. After one  
 251 second, however, the KM-GAP uptake is limited by bulk diffusion and slows down substantially.

252 After about one hour corresponding to  $\tau_{x_{\text{eff}}} (= \frac{x_{\text{eff}}^2}{D_b} = \frac{(20 \text{ nm})^2}{10^{-15} \text{ cm}^2 \text{ s}^{-1}} = 4000 \text{ s})$ , KM-GAP converges

253 with the F-S approximation using  $\alpha = \alpha_{\text{eff}} = \alpha(r_p/5) = 8 \times 10^{-4}$ . Notably, the F-S approximation with  
254  $\alpha_{\text{eff}}$  is identical to the MOSAIC approximation, although the latter is based on different rate  
255 equations using a unity mass accommodation coefficient like KM-GAP ( $\alpha_s = 1$ ) and a two-film  
256 approach of bulk diffusion (Zaveri et al., 2014). The MOSAIC transient solution exhibits a very  
257 high and likely overestimated initial uptake corresponding to the F-S approximation with  $\alpha = \alpha_s =$   
258 1, because it does not resolve reversible adsorption and desorption at the surface (Shiraiwa et al.,  
259 2012). After  $\sim 1$  min, however, the MOSAIC transient solution converges with KM-GAP. Overall,  
260 Figure 1 demonstrates that accurate modeling of SVOC partitioning and uptake into semisolid  
261 particles requires an explicit treatment of reversible adsorption and desorption at short time scales  
262 ( $< 1$  min) and an explicit treatment of bulk diffusion at intermediate time scales ( $\sim 1$  min to  $\sim 1$  h)  
263 when bulk concentration gradients evolve within the effective penetration depth. At long  
264 timescales ( $> \tau_{\text{eff}}$  of 1 h), the partitioning is reasonably well captured by both the MOSAIC  
265 approximation using a two-film approach of bulk diffusion (Zaveri et al., 2014) as well as the  
266 simple F-S approximation accounting for the influence of penetration depth with the effective mass  
267 accommodation coefficient,  $\alpha_{\text{eff}}$ , newly introduced this study.

268 Figure 2a shows the temporal evolution of the gas-phase concentration of organic  
269 compounds with different volatilities ( $C^0 = 0.1$  to  $1000 \mu\text{g m}^{-3}$ ) that undergo non-reactive  
270 partitioning into semisolid seed aerosol particles ( $D_b = 10^{-15} \text{ cm}^2 \text{ s}^{-1}$ ). At short timescales,  
271 substantial deviations can occur for semi-volatile compounds ( $C^0 = 1$  to  $100 \mu\text{g m}^{-3}$ ), but at longer  
272 time scales KM-GAP and the F-S approximation with  $\alpha_{\text{eff}}$  are in reasonably good agreement  
273 (relative deviations  $< 10\%$  after  $\sim 1$  h). For low-volatile compounds ( $C^0 < 1 \mu\text{g m}^{-3}$ ), equilibration  
274 is achieved faster than for semi-volatile compounds because local thermodynamic equilibrium  
275 between the gas phase and the particle surface is quickly established by condensation without  
276 significant re-evaporation (Li and Shiraiwa, 2019; Zaveri et al., 2014). Semi-volatile compounds  
277 with reactive functional groups can undergo particle-phase reactions such as dimerization and  
278 oligomerization (Ziemann and Atkinson, 2012). Peroxide-containing highly oxidized molecules  
279 (HOM) are labile with chemical half-lives shorter than one hour (Krapf et al., 2016; Tong et al.,  
280 2019) corresponding to  $k_b > \sim 2 \times 10^{-4}$ , and a recent study has shown that particle-phase reactions  
281 must be considered to describe HOM effects on particle growth (Pospisilova et al., 2020). First-  
282 order decomposition rate coefficients for organic hydroperoxides in SOA were reported in the

283 range of  $10^{-6} - 1.5 \times 10^{-3}$  (Tong et al., 2016; Tong et al., 2018; Wei et al., 2020) and can be enhanced  
284 by photolysis (Badali et al., 2015; Epstein et al., 2014) or Fenton-like reactions in the presence of  
285 transition metal ions (Goldstein and Meyerstein, 1999). Model results for SVOC partitioning plus  
286 reactive uptake with different rate coefficients in semisolid aerosol particles are shown in Figure  
287 2b. The results of the Fuchs-Sutugin approximation with  $\alpha_{\text{eff}} = \alpha(x_{\text{eff}})$  and  $x_{\text{eff}}$  from Eq. 7 are  
288 identical to the MOSAIC approximate and transient solutions. The uptake predicted by KM-GAP  
289 is similar but slightly slower in case of high bulk reaction rate coefficients, which can be attributed  
290 to the influence of reversible adsorption and desorption at the surface. Additional simulations with  
291  $\alpha_s = 0.1$  confirm that the results of the Fuchs-Sutugin approximation with  $\alpha_{\text{eff}}$  and the MOSAIC  
292 approximate solution are identical, and that the results of KM-GAP and the MOSAIC transient  
293 solution are similar (Fig. S1).

294 For a given surface accommodation coefficient of  $\alpha_s = 1$ , which is likely a good  
295 approximation for SVOC on organic surfaces (Julin et al., 2014; Von Domaros et al., 2020),  
296 Figures 3a and 3b show how the effective mass accommodation coefficient  $\alpha_{\text{eff}}$  depends on  
297 volatility and bulk diffusivity as related to particle phase state and viscosity according to the  
298 Stokes-Einstein relation (Shiraiwa et al., 2011). In the liquid phase with high bulk diffusivity ( $D_b$   
299  $> 10^{-10} \text{ cm}^2 \text{ s}^{-1}$ ),  $\alpha_{\text{eff}}$  is essentially the same as  $\alpha_s$  independent of volatility ( $\alpha_{\text{eff}} \approx \alpha_s \approx 1$ ). With a  
300 decrease of bulk diffusivity in viscous or semisolid particles,  $\alpha_{\text{eff}}$  decreases substantially for SVOC  
301 ( $0.3 < C^0 < 300 \text{ } \mu\text{g m}^{-3}$ ) and so-called intermediate volatility organic compounds (IVOC;  $300 < C^0$   
302  $< 3 \times 10^6 \text{ } \mu\text{g m}^{-3}$ ) but not for LVOC ( $3 \times 10^{-4} < C^0 < 0.3 \text{ } \mu\text{g m}^{-3}$ ) and so-called extremely low-volatile  
303 organic compounds (ELVOC;  $C^0 < 3 \times 10^{-4} \text{ } \mu\text{g m}^{-3}$ ). The reason why compounds with higher  
304 volatility are more strongly affected by particle phase state and diffusivity is that they are more  
305 likely to desorb back to the gas phase when diffusion into the bulk is slow. Compounds with lower  
306 volatility exhibit much lower desorption rates and are less likely to re-evaporate even if their  
307 diffusion into the bulk is slow. On the other hand, the influence of particle phase state and  
308 diffusivity increases with particle size because longer pathways of diffusion are required for  
309 effective accommodation, penetration, and absorption of gas molecules into larger particles as  
310 illustrated in Figures 3c and 3d.

311 The theoretically predicted influence of volatility on effective mass accommodation is  
312 consistent with a recent experimental study of  $\alpha$ -pinene SOA reporting that the observed mass  
313 accommodation coefficients decreased from  $\sim 1$  for low-volatile compounds to  $\sim 0.3$  for semi-

314 volatile compounds (Liu et al., 2019). Particle viscosity and bulk diffusivity were not reported for  
315 these experiments, but values around  $10^{-13}$  to  $10^{-14}$   $\text{cm}^2 \text{s}^{-1}$  had previously been estimated for the  
316 diffusion coefficient of organic compounds in  $\alpha$ -pinene SOA under dry conditions (Zhou et al.,  
317 2013). As illustrated in Figure 4a, theoretical predictions of  $\alpha_{\text{eff}}$  using Eqs. 5 & 6 under the  
318 assumption of quasi-steady-state conditions with  $\alpha_s = 1$  and  $D_b = 10^{-12}$  to  $10^{-14}$   $\text{cm}^2 \text{s}^{-1}$  can  
319 approximately capture the decrease and encompass the variability and uncertainty range of the  
320 experimentally derived mass accommodation coefficients reported by (Liu et al., 2019). Indeed,  
321 the observational  $\alpha_m$  values reported in (Liu et al., 2019) and other experimental studies are usually  
322 obtained by fitting measurement data with the F-S approximation, and thus they should be directly  
323 compared to effective mass accommodation coefficient  $\alpha_{\text{eff}}$  as derived by integration of the F-S  
324 approximation with detailed kinetic models of mass transport across the gas-particle interface.  
325 Figure 4b shows a wide range of other measurement-derived mass accommodation coefficients for  
326 various SOA and surrogate systems (data points/shaded areas) in comparison to generic values of  
327  $\alpha_{\text{eff}}$  (lines) calculated for characteristic experimental conditions ( $\omega = 2.0 \times 10^4$   $\text{cm s}^{-1}$ ,  $\rho_p = 1$   $\text{g cm}^{-3}$ ,  
328 and  $r_p = 100$   $\text{nm}$ , and  $D_b = 10^{-19}$  to  $10^{-5}$   $\text{cm}^2 \text{s}^{-1}$ ). As indicated by molecular dynamics simulations  
329 and related studies, the surface accommodation coefficient (adsorption probability) for semi-  
330 volatile or low-volatile organic compounds on organic surfaces is likely close to unity,  $\alpha_s = 1$  (Julin  
331 et al., 2014; Von Domaros et al., 2020). Accordingly, low observational values of  $\alpha$  can be  
332 attributed to the penetration-depth dependence of mass accommodation and plausibly explained  
333 by different scenarios/combinations/ratios of volatility and diffusivity, which can lead to a  
334 substantial decrease of  $\alpha_{\text{eff}}$  relative to  $\alpha_s$  in semi-solid particles. With regard to the dependence of  
335  $\alpha_{\text{eff}}$  on  $C^0$ , mixing effects and non-ideality may lead to deviations between  $C^0$  and  $C^*$  (Zuend and  
336 Seinfeld, 2012), which should be taken into account in further investigations of mass  
337 accommodation and its influence on the formation and growth of SOA particles.

338 On the other hand, high reactivity can compensate the influence of low diffusivity and mass  
339 transport limitations in the particle phase, keeping  $\alpha_{\text{eff}}$  close to  $\alpha_s$ . In case of non-reactive  
340 partitioning, the effective penetration depth used to calculate  $\alpha_{\text{eff}}$  is one fifth of the particle radius,  
341 i.e.,  $x_{\text{eff}}/r_p = 0.2$  (Eq. 6). In case of reactive uptake, however,  $x_{\text{eff}}$  decreases with increasing  
342 reactivity and with decreasing diffusivity according to Eqs. (7) to (9). Figure 5a illustrates how the  
343 effective penetration depth normalized by particle radius,  $x_{\text{eff}}/r_p$ , decreases with increasing first-

344 order bulk reaction rate coefficient,  $k_b$ , and with decreasing diffusion coefficient,  $D_b$ . The reduced  
345 effective penetration depths at high  $k_b$  and low  $D_b$  reflect that reactive uptake by semisolid particles  
346 proceeds mainly through chemical reaction near the surface (Shiraiwa et al., 2013a). Figure 5b  
347 illustrates how  $\alpha_{\text{eff}}$  depends on volatility and diffusivity for reactive uptake with  $\alpha_s = 1$  and a first-  
348 order bulk reaction rate coefficient  $k_b = 0.1 \text{ s}^{-1}$ . In comparison to Fig. 3b for non-reactive  
349 partitioning, Fig. 5b shows that particle phase reactivity leads to an extension of the volatility-  
350 diffusivity parameter space where  $\alpha_{\text{eff}} \approx \alpha_s$  (red area): For semi-solid particles with low diffusivity,  
351 the parameter range of strong deviations between  $\alpha_{\text{eff}}$  and  $\alpha_s$  (yellow/green/blue area) is shifted  
352 towards higher volatility (lower right corner).

353

#### 354 4. Summary and conclusions

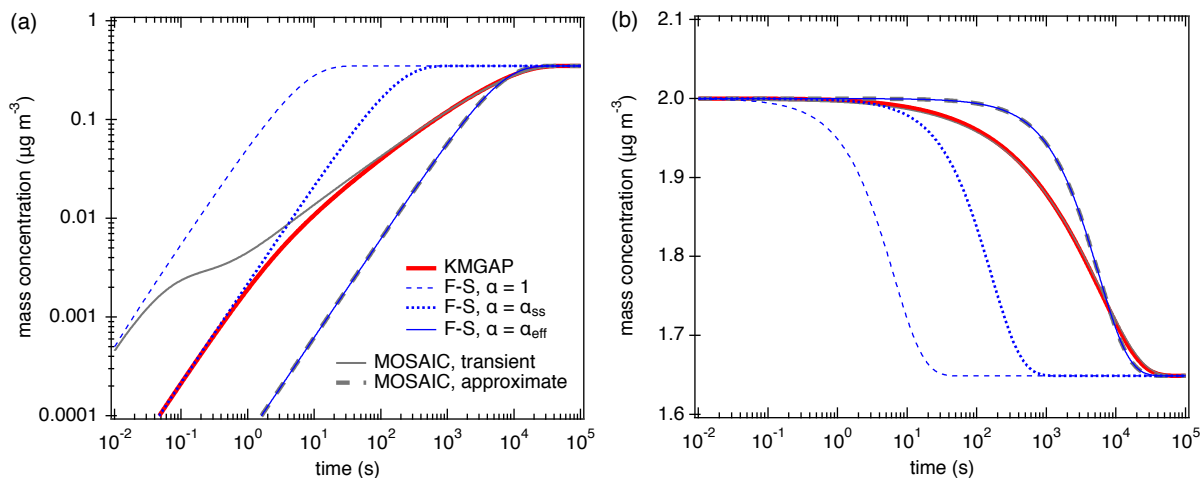
355 Traditional SOA modeling approaches are often using the Fuchs-Sutugin approximation of  
356 mass-transport kinetics at the gas-particle interface in combination with mass accommodation  
357 coefficients that are not appropriately defined, leading to inconsistent results and conclusions. To  
358 overcome such deficiencies and difficulties, we have introduced an effective mass accommodation  
359 coefficient  $\alpha_{\text{eff}}$  that depends on penetration depth and is a function of surface accommodation  
360 coefficient, volatility, bulk diffusivity, and particle-phase reaction rate coefficient. Application of  
361  $\alpha_{\text{eff}}$  in the traditional F-S approximation of SOA partitioning yields results that are consistent with  
362 detailed kinetic multilayer models (KM-GAP; Shiraiwa et al., 2012) and two-film models  
363 (MOSAIC, Zaveri et al., 2014)).

364 We suggest that  $\alpha_{\text{eff}}$  and its dependence on penetration depth and related parameters should  
365 be applied and considered when the F-S approximation is used to investigate and simulate gas-  
366 particle interactions in viscous or semi-solid organic aerosols. The simple parameterization can be  
367 incorporated into regional and global models for a more realistic representation of SOA processes  
368 in the atmosphere. *While kinetic limitations of bulk diffusion may not be critical for partitioning  
369 into liquid particles in the planetary boundary layer (PBL) at high relative humidity and high  
370 temperature, their effects are important for amorphous semi-solid or glassy particles predicted for  
371 the free and upper troposphere (FT/UT) as well as for the PBL at low relative humidity and low  
372 temperature (Andreae et al., 2018; Maclean et al., 2017; Shiraiwa et al., 2017). Following up on  
373 the helpful comments of an anonymous reviewer (Referee, 2020), we would like to emphasize that  
374 the effective mass accommodation coefficient offers a very efficient way of properly treating gas-*

375 particle partitioning in large-scale models, because it is easily applicable for liquid, semi-solid,  
376 and solid particles as function of standard physicochemical parameters.

377 In the analysis and interpretation of SOA chamber and laboratory experiments,  $\alpha_{\text{eff}}$   
378 provides a simply way of accounting for the potential impact of volatility, diffusivity, and particle  
379 phase state on the kinetics of gas-particle partitioning for analysis and interpretation of chamber  
380 experiments. In particular, it may help to address and resolve apparent inconsistencies between the  
381 definitions and parameter values of mass accommodation coefficients that are derived from  
382 experimental data and from molecular dynamics simulations.

383 At short timescales, before molecules diffuse to the effective penetration depth, however,  
384  $\alpha_{\text{eff}}$  is not sufficient to properly describe the kinetics of gas-particle interactions with the F-S  
385 approximation. The timescales to reach a quasi-steady state in the particle phase can be long (hours  
386 to days) for ultra-viscous and glassy phase states, low particle-phase reaction rate coefficients, and  
387 large particles (Shiraiwa et al., 2011; Zaveri et al., 2014). Such conditions require detailed kinetic  
388 model simulations with kinetic multilayer models or equivalent approaches explicitly resolving  
389 mass transport at the surface and in the bulk of the particle. The same applies for particles with  
390 layered structures such as surface crusts (solid/viscous surface layers) that may form upon  
391 chemical aging and can strongly impact the uptake of semi-volatile compounds and multiphase  
392 chemical processes in the particle phase (Pfrang et al., 2011; Vander Wall et al., 2018; Zhou et al.,  
393 2019). Moreover, mixed organic-inorganic particles often undergo liquid-liquid phase separation  
394 at moderate and high RH (Krieger et al., 2012; You et al., 2014; Zuend and Seinfeld, 2012), and  
395 liquid-liquid phase separation can also occur for purely organic particles (Song et al., 2017). For  
396 such particles with shell-core morphology, the effective penetration depth would be confined to  
397 particle shells, which could be smaller than the penetration depth estimated from the particle  
398 radius. The interplay of particle phase state and phase separation can further impact SOA  
399 partitioning (Shiraiwa et al., 2013b). In such complex particle morphologies with multiple phases,  
400 gradients and discontinuities of diffusivity may occur within the particle bulk and require more  
401 advanced modeling approaches of gas-particle interaction kinetics to be addressed in future  
402 studies.



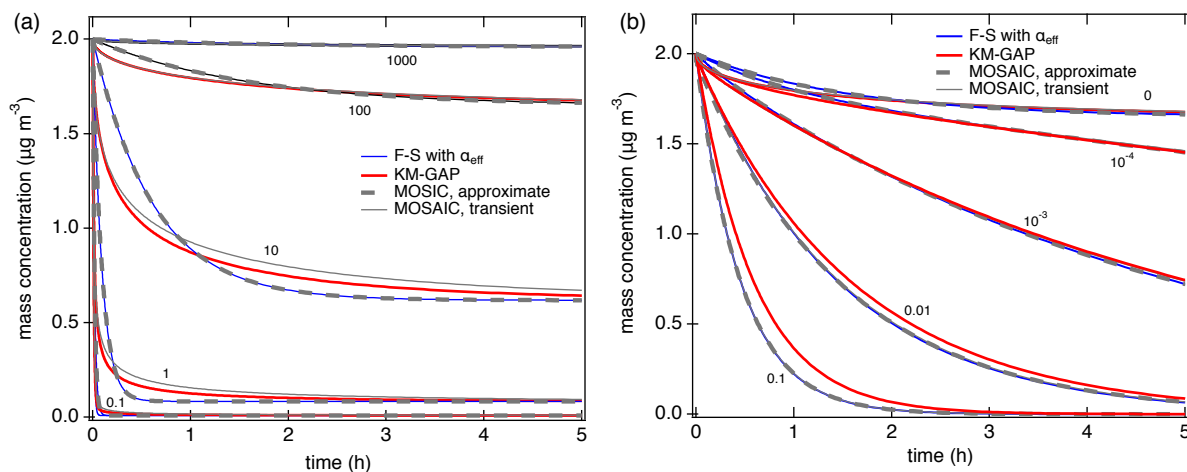
403

404

405 **Figure 1.** Temporal evolution of the particle phase concentration (a) and the gas phase  
 406 concentration (b) of semi-volatile organic compounds (SVOC,  $C^0 = 100 \mu\text{g m}^{-3}$ ) interacting with  
 407 semisolid seed aerosol particles ( $D_b = 10^{-15} \text{ cm}^2 \text{ s}^{-1}$ ,  $\omega = 2 \times 10^4 \text{ cm s}^{-1}$ ,  $\rho_p = 1 \text{ g cm}^{-3}$ ). The red lines  
 408 are simulation results of KM-GAP, and the blue lines are the results of an aerosol dynamic model  
 409 that employs the Fuchs-Sutugin approximation with  $\alpha = \alpha_s = 1$  (dashed),  $\alpha = \alpha_{ss} = 3 \times 10^{-2}$  (dotted),  
 410 and  $\alpha = \alpha_{eff} = 8 \times 10^{-4}$  (solid). The gray lines represent the MOSAIC transient solution (solid) and  
 411 approximate solution (dashed) (Zaveri et al., 2014).

412





413

414

415 **Figure 2.** Temporal evolution of the gas phase concentration of organic compounds interacting

416 with semisolid seed aerosol particles ( $\alpha_s = 1$ ,  $\omega = 2 \times 10^4 \text{ cm s}^{-1}$ ,  $D_b = 10^{-15} \text{ cm}^2 \text{ s}^{-1}$ ,  $\rho_p = 1 \text{ g cm}^{-3}$ ):

417 (a) Non-reactive partitioning of compounds with different volatilities ( $C^0 = 0.1, 1, 10, 100, 1000$

418  $\mu\text{g m}^{-3}$ ); (b) reactive uptake of semi-volatile compounds ( $C^0 = 100 \mu\text{g m}^{-3}$ ) with different first-

419 order bulk reaction rate coefficients ( $k_b = 0, 10^{-4}, 10^{-3}, 0.01, 0.1 \text{ s}^{-1}$ ). The red lines are simulation

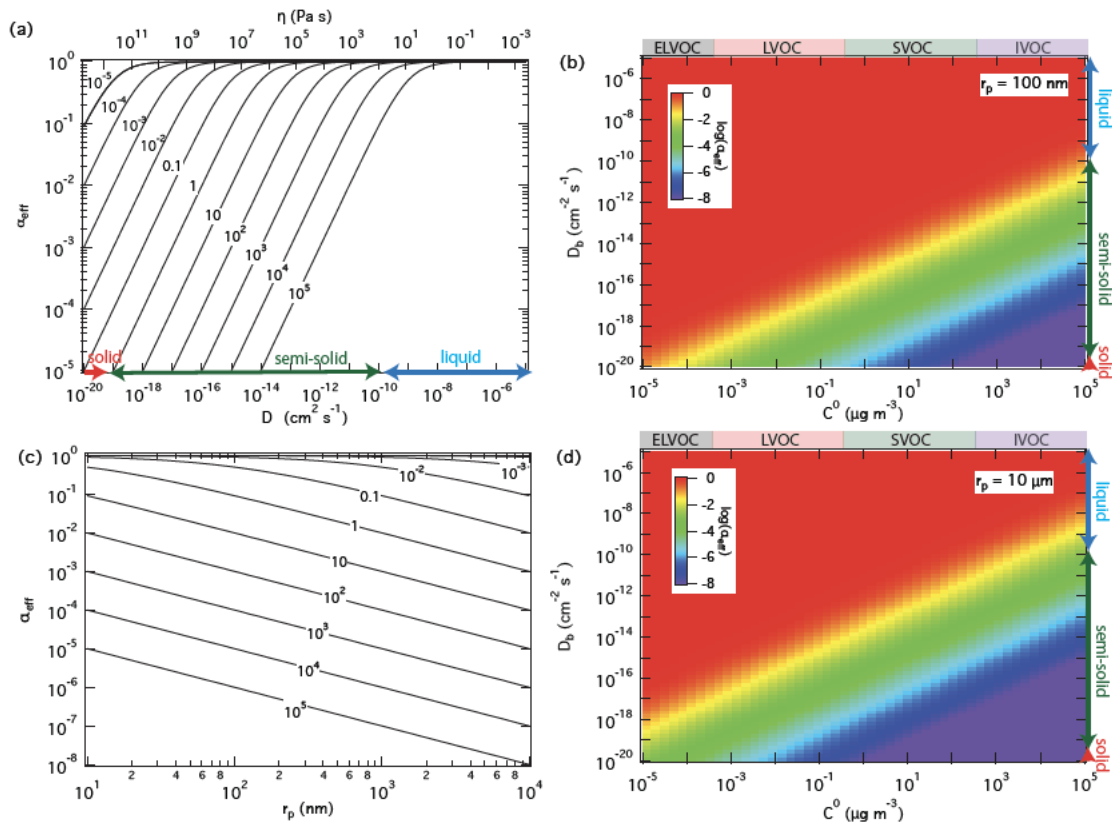
420 results of KM-GAP, and the blue lines are the results of an aerosol dynamic model that employs

421 the Fuchs-Sutugin approximation with  $\alpha_{\text{eff}} = \alpha(r_p/5)$  for non-reactive partitioning (a) and with  $\alpha_{\text{eff}}$

422  $= \alpha(x_{\text{eff}})$  and  $x_{\text{eff}}$  from Eq. (5) for reactive uptake (b). The gray lines represent the MOSAIC

423 transient solution (solid) and approximate solution (dashed) (Zaveri et al., 2014).

424



425

426

427 **Figure 3.** Effective mass accommodation coefficients,  $\alpha_{\text{eff}}$ , for non-reactive partitioning of organic

428 compounds Z ( $\alpha_s = 1$ ,  $\omega = 2 \times 10^4 \text{ cm s}^{-1}$ ) with liquid, semi-solid, or solid aerosol particles ( $\rho_p = 1$

429  $\text{g cm}^{-3}$ ) depending on pure compound volatility,  $C^0$ , particle bulk diffusivity,  $D_b$  (corresponding to

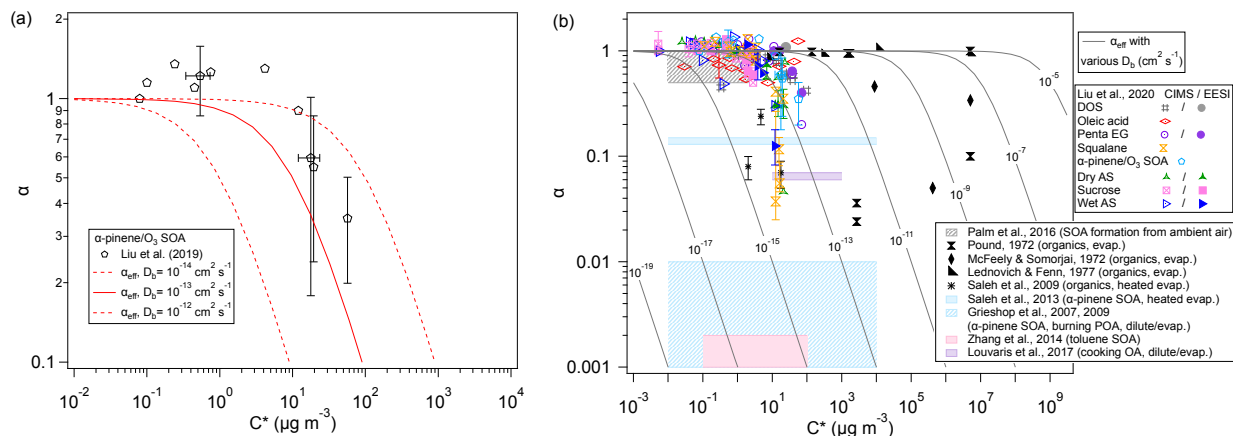
430 viscosity,  $\eta$ ), and particle radius,  $r_p$ :  $\alpha_{\text{eff}}$  calculated as a function of  $D_b$  for  $C^0 = 10^{-5}$  to  $10^5 \mu\text{g m}^{-3}$

431 with  $r_p = 100 \text{ nm}$  (a);  $\alpha_{\text{eff}}$  calculated as a function of  $C^0$  and  $D_b$  with  $r_p = 100 \text{ nm}$  (b) and  $10 \mu\text{m}$

432 (d);  $\alpha_{\text{eff}}$  calculated as a function of particle radius for  $D_b = 10^{-15} \text{ cm}^2 \text{ s}^{-1}$  and different levels of

433 volatility ( $C^0 = 10^{-3}$  to  $10^5 \mu\text{g m}^{-3}$ ) (c).

434



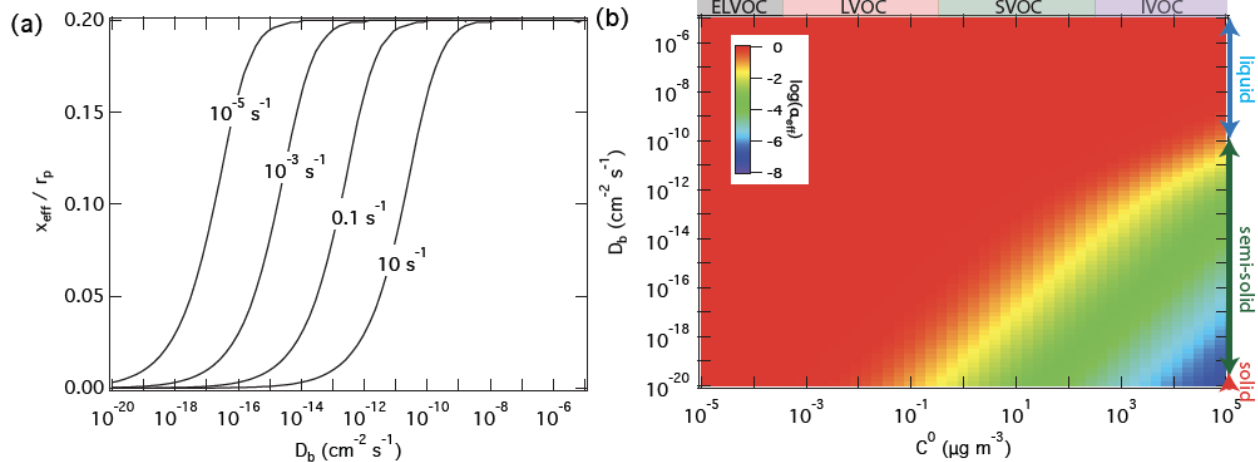
435

436

437 **Figure 4.** Effective mass accommodation coefficients,  $\alpha_{\text{eff}}$  (lines, Eqs. 5-10) compared to  
 438 measurement-derived mass accommodation coefficients,  $\alpha$  (data points/shaded areas, Eqs. 1-2),  
 439 plotted against effective saturation mass concentration,  $C^*$ , for various SOA and surrogate systems  
 440 assuming  $\alpha_s = 1$ ,  $\omega = 2 \times 10^4 \text{ cm s}^{-1}$ ,  $\rho = 1 \text{ g cm}^{-3}$ ,  $r_p = 100 \text{ nm}$ , and  $C^0 = C^*$ : (a) observational  
 441 results from laboratory experiments with semi-volatile components of SOA generated by  
 442 ozonolysis of  $\alpha$ -pinene (data points, (Liu et al., 2019)) compared to  $\alpha_{\text{eff}}$  for  $D_b = 10^{-14}$  to  $10^{-12} \text{ cm}^2$   
 443  $\text{s}^{-1}$  (lines); (b) observational results from earlier experimental investigations of laboratory-  
 444 generated and ambient samples (data points/shaded areas, compiled by Liu et al., 2019) compared  
 445 to generic values of  $\alpha_{\text{eff}}$  for  $D_b = 10^{-19}$  to  $10^{-5} \text{ cm}^2 \text{ s}^{-1}$  (lines).

446

447



448

449

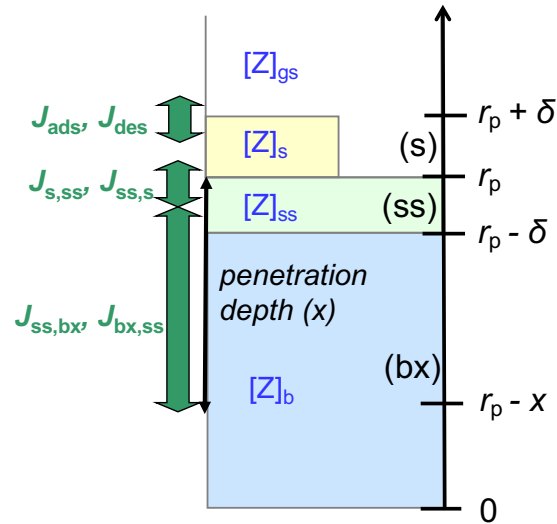
450 **Figure 5.** Effective penetration depths normalized by particle radius,  $x_{\text{eff}}$ , and mass  
451 accommodation coefficients,  $\alpha_{\text{eff}}$ , for reactive uptake of organic compounds  $Z$  ( $\alpha_s = 1$ ,  $\omega = 2 \times 10^4$   
452  $\text{cm s}^{-1}$ ) by liquid, semi-solid, or solid aerosol particles ( $r_p = 100 \text{ nm}$ ,  $\rho_p = 1 \text{ g cm}^{-3}$ ) depending on  
453 pure compound volatility,  $C^0$ , particle bulk diffusivity  $D_b$ , and first-order bulk reaction rate  
454 coefficient,  $k_b$ : (a)  $x_{\text{eff}}$  calculated as a function of  $D_b$  and  $k_b = 10^{-5}$  to  $10 \text{ s}^{-1}$ ; (b)  $\alpha_{\text{eff}}$  calculated as a  
455 function of  $C^0$  and  $D_b$  for  $k_b = 0.1 \text{ s}^{-1}$ .

456

457

458 **Appendix:**

459 **Derivation of penetration-depth-dependent mass accommodation coefficient**



460

461 **Figure A1.** Schematic illustration of the kinetic multilayer modelling approach resolving mass  
 462 transport fluxes ( $J$ ) between the near-surface gas phase (gs), the sorption layer (s), the quasi-static  
 463 surface layer (ss), and the bulk layer at penetration depth  $x$  (bx) (Shiraiwa et al., 2012).

464

465 Figure A1 illustrates the applied kinetic multi-layer model framework, in which the  
 466 structure and composition of a particle are described by a sorption layer (s), a quasi-static surface  
 467 layer (ss), multiple bulk layers (b), and any volatile, semi-volatile, or low-volatile chemical species  
 468 ( $Z$ ) that can undergo gas-particle partitioning and transport between the different layers and  
 469 chemical reactions with each other (Pöschl et al., 2007; Shiraiwa et al., 2012). At low gas-phase  
 470 concentration levels or high surface bulk exchange rates (e.g., for liquid particles under dilute  
 471 atmospheric conditions), surface coverage and saturation effects can be neglected, and the surface  
 472 accommodation coefficient ( $\alpha_s$ ) approaches the parameter value for an adsorbate-free surface ( $\alpha_s$   
 473  $\approx \alpha_{s,0}$ ) (Pöschl et al., 2007; Shiraiwa et al., 2012). In the absence of condensed-phase reactions, a  
 474 quasi-static surface accommodation coefficient ( $\alpha_{ss}$ ), i.e. the probability for a gas molecule  
 475 colliding with the surface to enter the quasi-static surface layer, can be calculated as follows  
 476 (Shiraiwa et al., 2012):

477

$$\alpha_{ss} = \alpha_s \frac{J_{s,ss}}{J_d + J_{s,ss}} = \alpha_s \frac{k_{s,ss}}{k_d + k_{s,ss}} \quad (\text{A1})$$

478 Here  $J_d$  is the desorption flux of Z and  $k_d$  is the corresponding first-order rate coefficient;  $J_{s,ss}$  and  
 479  $k_{s,ss}$  represent the flux and first-order rate coefficient of transfer between the sorption layer and the  
 480 quasi-static surface layer. The probability for an individual gas molecule colliding with the surface  
 481 to enter the bulk with a penetration depth  $x$  can be described by a penetration depth-dependent  
 482 mass accommodation coefficient,  $\alpha(x)$ , defined as follows:

$$483 \quad \alpha(x) = \alpha_{ss} \frac{\Psi_{ss,bx}}{1 - \Psi_{ss,s} \Psi_{s,ss}} \quad (A2)$$

484 Here  $\Psi_{s,ss}$  is the probability for Z in the sorption layer to enter the quasi-static surface layer and  
 485  $\Psi_{ss,bx}$  and  $\Psi_{ss,s}$  are the probabilities for Z in the quasi-static surface layer to enter the bulk with the  
 486 penetration depth of  $x$  or the sorption layer, respectively, which are determined by the  
 487 corresponding fluxes and first-order rate coefficients of mass transport (Shiraiwa et al., 2012):

$$488 \quad \Psi_{s,ss} = J_{s,ss} / (J_{s,ss} + J_{des}) = k_{s,ss} / (k_{s,ss} + k_d) \quad (A3)$$

$$489 \quad \Psi_{ss,s} = J_{ss,s} / (J_{ss,bx} + J_{ss,s}) = k_{ss,s} / (k_{ss,bx} + k_{ss,s}) \quad (A4)$$

$$490 \quad \Psi_{ss,bx} = J_{ss,bx} / (J_{ss,bx} + J_{ss,s}) = k_{ss,bx} / (k_{ss,bx} + k_{ss,s}) \quad (A5)$$

491 Inserting Eqs. (A3)-(A5) in Eq. (A2) leads to:

$$493 \quad \alpha(x) = \alpha_s \frac{k_{s,ss}}{k_d + k_{s,ss}} \frac{\frac{k_{ss,bx}}{k_{ss,bx} + k_{ss,s}}}{1 - \frac{k_{ss,s}}{k_{ss,bx} + k_{ss,s}} \cdot \frac{k_{s,ss}}{k_{s,ss} + k_d}}$$

$$494 \quad = \alpha_s \frac{k_{s,ss} k_{ss,bx}}{(k_d + k_{s,ss})(k_{ss,bx} + k_{ss,s}) \left(1 - \frac{k_{ss,s}}{k_{ss,bx} + k_{ss,s}} \cdot \frac{k_{s,ss}}{k_{s,ss} + k_d}\right)}$$

$$495 \quad = \alpha_s \frac{k_{s,ss} k_{ss,bx}}{(k_d + k_{s,ss})(k_{ss,bx} + k_{ss,s}) - k_{ss,s} k_{s,ss}}$$

$$496 \quad = \alpha_s \frac{k_{s,ss} k_{ss,bx}}{k_d k_{ss,bx} + k_{s,ss} k_{ss,bx} + k_d k_{ss,s}} = \alpha_s \frac{1}{1 + \frac{k_d k_{ss,s} + k_d k_{ss,bx}}{k_{s,ss} k_{ss,bx}}}$$

$$497 \quad = \alpha_s \frac{1}{1 + \frac{k_d}{k_{s,ss}} \frac{k_{ss,s} + k_{ss,bx}}{k_{ss,bx}}} = \alpha_s \frac{1}{1 + \frac{k_d}{k_{s,ss}} \left(1 + \frac{k_{ss,s}}{k_{ss,bx}}\right)}$$

$$492 \quad (A6)$$

498 The first-order rate coefficients of adsorption and desorption are given by  $k_a = \alpha_s \omega / 4$  and  $k_d =$   
 499  $1/\tau_d$ , respectively, where  $\omega$  (cm s<sup>-1</sup>) is the mean thermal velocity of Z in the gas phase and  $\tau_d$  is the  
 500 lifetime of desorption from the sorption layer (Pöschl et al., 2007; Shiraiwa et al., 2012). The rate

501 coefficient of mass transfer between sorption layer and quasi-static surface layer can be estimated  
 502 based on the Fick's first law of diffusion considering that a molecule in the sorption layer needs to  
 503 travel a distance of  $\delta$  to move into the quasi-static surface layer:  $k_{s,ss} \approx D_b / \delta^2$  (Shiraiwa et al.,  
 504 2012). An estimate for  $k_{s,ss}$  can be determined considering mass transport under equilibrium  
 505 conditions, where mass balance implies  $J_{s,ss} = J_{ss,s}$ , i.e.,  $k_{s,ss} [Z]_{s,eq} = k_{ss,s} [Z]_{ss,eq}$ , and  $J_{des} = J_{ads}$ , i.e.,  
 506  $k_d [Z]_{s,eq} = k_a [Z]_{g,eq}$  (Shiraiwa et al., 2012). Here  $[Z]_{g,eq}$ ,  $[Z]_{s,eq}$ , and  $[Z]_{ss,eq}$  are the equilibrium or  
 507 solubility saturation number concentrations of Z in the gas phase, on the sorption layer, and in the  
 508 quasi-static surface layer, respectively:

$$509 \quad k_{s,ss} = k_{ss,s} \frac{k_d [Z]_{ss,eq}}{k_a [Z]_{g,eq}} \quad (A7)$$

$$510 \quad \frac{k_d}{k_{s,ss}} = \frac{k_a [Z]_{g,eq}}{k_{ss,s} [Z]_{ss,eq}} = \frac{k_a [Z]_{g,eq}}{k_{ss,s} [Z]_{b,eq} \delta} \quad (A8)$$

511  
 512 In analogy, the first-order rate coefficient  $k_{bx,ss}$  can be estimated based on the Fick's first law of  
 513 diffusion, considering that a molecule Z at penetration depth  $x$  in the bulk needs to travel a distance  
 514 of  $x - \delta$  to move into the quasi-static surface layer (Fig. A1):  $k_{bx,ss} \approx D_b / (x - \delta)$ . Under equilibrium  
 515 conditions,  $J_{ss,bx} = J_{bx,ss}$  and  $k_{ss,bx} [Z]_{ss,eq} = k_{bx,ss} [Z]_{b,eq}$  which leads to  $k_{ss,bx} = k_{bx,ss} / \delta = D_b / (\delta(x - \delta))$   
 516 assuming ideal mixing conditions and  $[Z]_{b,eq} = [Z]_{ss,eq} / \delta$  (Shiraiwa et al., 2012). Thus,  $k_{ss,s} / k_{ss,bx} =$   
 517  $(D_b / \delta^2) / (D_b / (\delta(x - \delta))) = (x - \delta) / \delta$ .

518 Based on the absorptive partitioning theory (Donahue et al., 2006; Pankow, 1994),

$$519 \quad C^0 = \frac{C^g}{C^p} C_{OA} \quad (A9)$$

520  
 521 where  $C^0$  ( $\mu\text{g m}^{-3}$ ) is the pure compound saturation mass concentration,  $C^g$  and  $C^p$  ( $\mu\text{g m}^{-3}$ ) are the  
 522 gas-phase and particle-phase mass concentrations of the compound Z, respectively, and  $C_{OA}$  ( $\mu\text{g}$   
 523  $\text{m}^{-3}$ ) is the total organic aerosol mass concentration.  $C^g$  and  $[Z]_{g,eq}$  are related through the following  
 524 equation:

$$525 \quad C^g = \frac{[Z]_{g,eq} M}{N_A} \cdot 10^{12} \frac{\mu\text{g m}^{-3}}{\text{g cm}^{-3}} \quad (A10)$$

526 where  $M$  is the molar mass of compound Z.  $[Z]_{g,eq}$  is the equilibrium (saturation) number  
 527 concentration of Z in the gas phase.  $[Z]_{g,eq}$  can be calculated using the saturation vapor pressure  $p$ :

528  $[Z]_{g,eq} = p N_A / (R T)$  where  $N_A$  is the Avogadro number,  $R$  is the gas constant, and  $T$  is the  
 529 temperature.  $[Z]_{b,eq}$  corresponds to the ratio between the number concentration of  $Z$  in the particle  
 530 phase (per  $m^3$  of air) to the particle volume concentration ( $m^3$  per  $m^3$  of air), which can be  
 531 expressed using  $C_Z^{PM}$  and  $C_{OA}$  with the particle density  $\rho_P$  ( $g\ cm^{-3}$ ):

$$532 \quad [Z]_{b,eq} = \frac{\frac{C^P}{M} N_A}{\frac{C_{OA}}{\rho}} = \frac{C^P N_A \rho_P}{C_{OA} M} \quad (A11)$$

533 Combining Eq. (A9) – (A11) would lead to:

$$534 \quad \frac{[Z]_{g,eq}}{[Z]_{b,eq}} = \frac{\frac{C^g N_A}{M}}{\frac{C^P N_A \rho_P}{C_{OA} M}} \cdot 10^{-12} = \frac{C^g}{C^P} C_{OA} \frac{1}{\rho_P} \cdot 10^{-12} = \frac{C^0}{\rho_P} \cdot 10^{-12} \frac{g\ cm^{-3}}{\mu g\ m^{-3}} \quad (A12)$$

535 Inserting Eq. (A8) into Eq. (A6) and combination with Eq. (A12) leads to:

$$536 \quad \alpha(x) = \alpha_s \frac{1}{1 + \frac{k_a}{k_{ss,s}} \frac{[Z]_{g,eq}}{[Z]_{b,eq}} \delta \left(1 + \frac{x - \delta}{\delta}\right)} = \alpha_s \frac{1}{1 + \frac{\alpha_s \omega C^0}{4 D_b \rho_P} x \cdot 10^{-12} \frac{g\ cm^{-3}}{\mu g\ m^{-3}}} \quad (A13)$$

537  
 538 **Acknowledgements.** MS acknowledges funding by the National Science Foundation (AGS-  
 539 1654104) and the Department of Energy (DE-SC0018349). We thank Jose Jimenez (CU Boulder)  
 540 for stimulating discussions and for sharing published data and experimental information as  
 541 presented in Figure 4. [Moreover, we thank two anonymous reviewers for helpful comments and](#)  
 542 [discussions.](#)

543  
 544 **Author contributions.** MS and UP designed the study, analyzed the data, and wrote the paper.  
 545 MS conducted kinetic modeling.

546  
 547 **Competing interests.** The authors declare that they have no conflict of interest.

548  
 549 **Data availability.** The simulation data may be obtained from the corresponding author upon  
 550 request.

551  
 552 **References.**



553 Alpert, P. A., Corral Arroyo, P., Dou, J., Krieger, U. K., Steimer, S. S., Förster, J.-D., Ditas, F.,  
554 Pöhlker, C., Rossignol, S., Passananti, M., Perrier, S., George, C., Shiraiwa, M., Berkemeier, T.,  
555 Watts, B. and Ammann, M.: Visualizing reaction and diffusion in xanthan gum aerosol particles  
556 exposed to ozone, *Phys. Chem. Chem. Phys.*, 21, 20613-20627, 10.1039/C9CP03731D, 2019.

557 Andreae, M. O., Afchine, A., Albrecht, R., Holanda, B. A., Artaxo, P., Barbosa, H. M. J.,  
558 Borrmann, S., Cecchini, M. A., Costa, A., Dollner, M., Fütterer, D., Järvinen, E., Jurkat, T.,  
559 Klimach, T., Konemann, T., Knote, C., Krämer, M., Krisna, T., Machado, L. A. T., Mertes, S.,  
560 Minikin, A., Pöhlker, C., Pöhlker, M. L., Pöschl, U., Rosenfeld, D., Sauer, D., Schlager, H.,  
561 Schnaiter, M., Schneider, J., Schulz, C., Spanu, A., Sperling, V. B., Voigt, C., Walser, A., Wang,  
562 J., Weinzierl, B., Wendisch, M. and Ziereis, H.: Aerosol characteristics and particle production in  
563 the upper troposphere over the Amazon Basin, *Atmos. Chem. Phys.*, 18, 921-961, 10.5194/acp-  
564 18-921-2018, 2018.

565 Aumont, B., Szopa, S. and Madronich, S.: Modelling the evolution of organic carbon during its  
566 gas-phase tropospheric oxidation: development of an explicit model based on a self generating  
567 approach, *Atmos. Chem. Phys.*, 5, 2497-2517, 10.5194/acp-5-2497-2005, 2005.

568 Badali, K. M., Zhou, S., Aljawhary, D., Antiñolo, M., Chen, W. J., Lok, A., Mungall, E., Wong,  
569 J. P. S., Zhao, R. and Abbatt, J. P. D.: Formation of hydroxyl radicals from photolysis of secondary  
570 organic aerosol material, *Atmos. Chem. Phys.*, 15, 7831-7840, 10.5194/acp-15-7831-2015, 2015.

571 Berkemeier, T., Steimer, S., Krieger, U. K., Peter, T., Poschl, U., Ammann, M. and Shiraiwa, M.:  
572 Ozone uptake on glassy, semi-solid and liquid organic matter and the role of reactive oxygen  
573 intermediates in atmospheric aerosol chemistry, *Phys. Chem. Chem. Phys.*, 18, 12662-12674,  
574 10.1039/C6CP00634E, 2016.

575 Berkemeier, T., Ammann, M., Krieger, U. K., Peter, T., Spichtinger, P., Pöschl, U., Shiraiwa, M.  
576 and Huisman, A. J.: Technical note: Monte Carlo genetic algorithm (MCGA) for model analysis  
577 of multiphase chemical kinetics to determine transport and reaction rate coefficients using multiple  
578 experimental data sets, *Atmos. Chem. Phys.*, 17, 8021-8029, 10.5194/acp-17-8021-2017, 2017.

579 Cappa, C. D., Jathar, S. H., Kleeman, M. J., Docherty, K. S., Jimenez, J. L., Seinfeld, J. H. and  
580 Wexler, A. S.: Simulating secondary organic aerosol in a regional air quality model using the  
581 statistical oxidation model - Part 2: Assessing the influence of vapor wall losses, *Atmos. Chem.*  
582 *Phys.*, 16, 3041-3059, 10.5194/acp-16-3041-2016, 2016.

583 Davies, J. F. and Wilson, K. R.: Nanoscale interfacial gradients formed by the reactive uptake of  
584 OH radicals onto viscous aerosol surfaces, *Chem. Sci.*, 6, 7020-7027, 2015.

585 Donahue, N. M., Robinson, A. L., Stanier, C. O. and Pandis, S. N.: Coupled partitioning, dilution,  
586 and chemical aging of semivolatile organics, *Environ. Sci. Technol.*, 40, 2635-2643,  
587 10.1021/es052297c, 2006.

588 Epstein, S. A., Blair, S. L. and Nizkorodov, S. A.: Direct photolysis of  $\alpha$ -pinene ozonolysis  
589 secondary organic aerosol: effect on particle mass and peroxide content, *Environ. Sci. Technol.*,  
590 48, 11251-11258, 2014.

591 Fowler, K., Connolly, P. J., Topping, D. O. and O'Meara, S.: Maxwell–Stefan diffusion: a  
592 framework for predicting condensed phase diffusion and phase separation in atmospheric aerosol,  
593 *Atmos. Chem. Phys.*, 18, 1629-1642, 10.5194/acp-18-1629-2018, 2018.

594 Goldstein, S. and Meyerstein, D.: Comments on the mechanism of the “Fenton-like” reaction, *Acc.*  
595 *Chem. Res.*, 32, 547-550, 1999.

596 Jathar, S. H., Cappa, C. D., Wexler, A. S., Seinfeld, J. H. and Kleeman, M. J.: Simulating  
597 secondary organic aerosol in a regional air quality model using the statistical oxidation model -  
598 Part 1: Assessing the influence of constrained multi-generational ageing, *Atmos. Chem. Phys.*, 16,  
599 2309-2322, 10.5194/acp-16-2309-2016, 2016.

600 Jimenez, J. L., Canagaratna, M. R., Donahue, N. M., Prevot, A. S. H., Zhang, Q., Kroll, J. H.,  
601 DeCarlo, P. F., Allan, J. D., Coe, H., Ng, N. L., Aiken, A. C., Docherty, K. S., Ulbrich, I. M.,  
602 Grieshop, A. P., Robinson, A. L., Duplissy, J., Smith, J. D., Wilson, K. R., Lanz, V. A., Hueglin,  
603 C., Sun, Y. L., Tian, J., Laaksonen, A., Raatikainen, T., Rautiainen, J., Vaattovaara, P., Ehn, M.,  
604 Kulmala, M., Tomlinson, J. M., Collins, D. R., Cubison, M. J., Dunlea, E. J., Huffman, J. A.,  
605 Onasch, T. B., Alfarra, M. R., Williams, P. I., Bower, K., Kondo, Y., Schneider, J., Drewnick, F.,  
606 Borrmann, S., Weimer, S., Demerjian, K., Salcedo, D., Cottrell, L., Griffin, R., Takami, A.,  
607 Miyoshi, T., Hatakeyama, S., Shimono, A., Sun, J. Y., Zhang, Y. M., Dzepina, K., Kimmel, J. R.,  
608 Sueper, D., Jayne, J. T., Herndon, S. C., Trimborn, A. M., Williams, L. R., Wood, E. C.,  
609 Middlebrook, A. M., Kolb, C. E., Baltensperger, U. and Worsnop, D. R.: Evolution of organic  
610 aerosols in the atmosphere, *Science*, 326, 1525-1529, 10.1126/science.1180353, 2009.

611 Julin, J., Winkler, P. M., Donahue, N. M., Wagner, P. E. and Riipinen, I. A.: Near unity mass  
612 accommodation coefficient of organic molecules of varying structure, *Environ. Sci. Technol.*, 48,  
613 12083–12089, 10.1021/es501816h, 2014.

614 Kanakidou, M., Seinfeld, J. H., Pandis, S. N., Barnes, I., Dentener, F. J., Facchini, M. C., Van  
615 Dingenen, R., Ervens, B., Nenes, A., Nielsen, C. J., Swietlicki, E., Putaud, J. P., Balkanski, Y.,  
616 Fuzzi, S., Horth, J., Moortgat, G. K., Winterhalter, R., Myhre, C. E. L., Tsigaridis, K., Vignati, E.,  
617 Stephanou, E. G. and Wilson, J.: Organic aerosol and global climate modelling: a review, *Atmos.*  
618 *Chem. Phys.*, 5, 1053-1123, 2005.

619 Knopf, D. A., Alpert, P. A. and Wang, B.: The Role of Organic Aerosol in Atmospheric Ice  
620 Nucleation: A Review, *ACS Earth Space Chem.*, 10.1021/acsearthspacechem.7b00120, 2018.

621 Kolb, C. E., Cox, R. A., Abbatt, J. P. D., Ammann, M., Davis, E. J., Donaldson, D. J., Garrett, B.  
622 C., George, C., Griffiths, P. T., Hanson, D. R., Kulmala, M., McFiggans, G., Pöschl, U., Riipinen,  
623 I., Rossi, M. J., Rudich, Y., Wagner, P. E., Winkler, P. M., Worsnop, D. R. and O' Dowd, C. D.:  
624 An overview of current issues in the uptake of atmospheric trace gases by aerosols and clouds,  
625 *Atmos. Chem. Phys.*, 10, 10561-10605, 10.5194/acp-10-10561-2010, 2010.

626 Koop, T., Bookhold, J., Shiraiwa, M. and Pöschl, U.: Glass transition and phase state of organic  
627 compounds: dependency on molecular properties and implications for secondary organic aerosols  
628 in the atmosphere, *Phys. Chem. Chem. Phys.*, 13, 19238-19255, 2011.

629 Kostenidou, E., Karnezi, E., Hite Jr, J. R., Bougiatioti, A., Cerully, K., Xu, L., Ng, N. L., Nenes,  
630 A. and Pandis, S. N.: Organic aerosol in the summertime southeastern United States: components  
631 and their link to volatility distribution, oxidation state and hygroscopicity, *Atmos. Chem. Phys.*,  
632 18, 5799-5819, 10.5194/acp-18-5799-2018, 2018.

633 Krapf, M., El Haddad, I., Bruns, Emily A., Molteni, U., Daellenbach, Kaspar R., Prévôt, André S.  
634 H., Baltensperger, U. and Dommen, J.: Labile Peroxides in Secondary Organic Aerosol, *Chem*, 1,  
635 603-616, 2016.

636 Krieger, U. K., Marcolli, C. and Reid, J. P.: Exploring the complexity of aerosol particle properties  
637 and processes using single particle techniques, *Chem. Soc. Rev.*, 41, 6631-6662,  
638 10.1039/c2cs35082c, 2012.

639 Kroll, J. H. and Seinfeld, J. H.: Chemistry of secondary organic aerosol: Formation and evolution  
640 of low-volatility organics in the atmosphere, *Atmos. Environ.*, 42, 3593-3624,  
641 10.1016/j.atmosenv.2008.01.003, 2008.

642 Kuwata, M. and Martin, S. T.: Phase of atmospheric secondary organic material affects its  
643 reactivity, *Proc. Natl. Acad. Sci. U.S.A.*, 109, 17354-17359, 10.1073/pnas.1209071109, 2012.

644 Lee, B. H., Kostenidou, E., Hildebrandt, L., Riipinen, I., Engelhart, G. J., Mohr, C., DeCarlo, P.  
645 F., Mihalopoulos, N., Prevot, A. S. H., Baltensperger, U. and Pandis, S. N.: Measurement of the  
646 ambient organic aerosol volatility distribution: application during the Finokalia Aerosol  
647 Measurement Experiment (FAME-2008), *Atmos. Chem. Phys.*, 10, 12149-12160, 10.5194/acp-  
648 10-12149-2010, 2010.

649 Li, Y. and Shiraiwa, M.: Timescales of secondary organic aerosols to reach equilibrium at various  
650 temperatures and relative humidities, *Atmos. Chem. Phys.*, 19, 5959-5971, 10.5194/acp-19-5959-  
651 2019, 2019.

652 Liu, P., Li, Y. J., Wang, Y., Gilles, M. K., Zaveri, R. A., Bertram, A. K. and Martin, S. T.: Lability  
653 of secondary organic particulate matter, *Proc. Natl. Acad. Sci. U.S.A.*, 113, 12643-12648, 2016.

654 Liu, X., Day, D. A., Krechmer, J. E., Brown, W., Peng, Z., Ziemann, P. J. and Jimenez, J. L.:  
655 Direct measurements of semi-volatile organic compound dynamics show near-unity mass  
656 accommodation coefficients for diverse aerosols, *Commun. Chem.*, 2, 98, 10.1038/s42004-019-  
657 0200-x, 2019.

658 Maclean, A. M., Butenhoff, C. L., Grayson, J. W., Barsanti, K., Jimenez, J. L. and Bertram, A. K.:  
659 Mixing times of organic molecules within secondary organic aerosol particles: a global planetary  
660 boundary layer perspective, *Atmos. Chem. Phys.*, 17, 13037-13048, 10.5194/acp-17-13037-2017,  
661 2017.

662 McVay, R. C., Cappa, C. D. and Seinfeld, J. H.: Vapor–Wall Deposition in Chambers: Theoretical  
663 Considerations, *Environ. Sci. Technol.*, 48, 10251-10258, 2014.

664 Mu, Q., Shiraiwa, M., Octaviani, M., Ma, N., Ding, A., Su, H., Lammel, G., Pöschl, U. and Cheng,  
665 Y.: Temperature effect on phase state and reactivity controls atmospheric multiphase chemistry  
666 and transport of PAHs, *Science Advances*, 4, eaap7314, 2018.

667 Pandis, S. N., Wexler, A. S. and Seinfeld, J. H.: Secondary organic aerosol formation and  
668 transport. 2. Predicting the ambient secondary organic aerosol - size distribution, *Atmos. Environ.*,  
669 27A, 2403-2416, 10.1016/0960-1686(93)90408-q, 1993.

670 Pankow, J. F.: An absorption model of gas-particle partitioning of organic-compounds in the  
671 atmosphere, *Atmos. Environ.*, 28, 185-188, 1994.

672 Perraud, V., Bruns, E. A., Ezell, M. J., Johnson, S. N., Yu, Y., Alexander, M. L., Zelenyuk, A.,  
673 Imre, D., Chang, W. L., Dabdub, D., Pankow, J. F. and Finlayson-Pitts, B. J.: Nonequilibrium  
674 atmospheric secondary organic aerosol formation and growth, *Proc. Natl. Acad. Sci. U.S.A.*, 109,  
675 2836-2841, 10.1073/pnas.1119909109, 2012.

676 Pfrang, C., Shiraiwa, M. and Pöschl, U.: Chemical ageing and transformation of diffusivity in  
677 semi-solid multi-component organic aerosol particles, *Atmos. Chem. Phys.*, 11, 7343-7354,  
678 10.5194/acp-11-7343-2011, 2011.

679 Pöschl, U., Rudich, Y. and Ammann, M.: Kinetic model framework for aerosol and cloud surface  
680 chemistry and gas-particle interactions - Part 1: General equations, parameters, and terminology,  
681 *Atmos. Chem. Phys.*, 7, 5989-6023, 2007.

682 Pöschl, U. and Shiraiwa, M.: Multiphase Chemistry at the Atmosphere–Biosphere Interface  
683 Influencing Climate and Public Health in the Anthropocene, *Chem. Rev.*, 115, 4440–4475,  
684 10.1021/cr500487s, 2015.

685 Pospisilova, V., Lopez-Hilfiker, F. D., Bell, D. M., El Haddad, I., Mohr, C., Huang, W., Heikkinen,  
686 L., Xiao, M., Dommen, J., Prevot, A. S. H., Baltensperger, U. and Slowik, J. G.: On the fate of  
687 oxygenated organic molecules in atmospheric aerosol particles, *Science Advances*, 6, eaax8922,  
688 10.1126/sciadv.aax8922, 2020.

689 Referee: Interactive comment on “Mass Accommodation and Gas-Particle Partitioning in  
690 Secondary Organic Aerosols: Dependence on Diffusivity, Volatility, Particle-phase Reactions, and  
691 Penetration Depth” by Manabu Shiraiwa and Ulrich Pöschl, *Atmos. Chem. Phys. Discuss.*,  
692 <https://doi.org/10.5194/acp-2020-5536-RC5192>, 2020.

693 Reid, J. P., Bertram, A. K., Topping, D. O., Laskin, A., Martin, S. T., Petters, M. D., Pope, F. D.  
694 and Rovelli, G.: The viscosity of atmospherically relevant organic particles, *Nat. Commun.*, 9,  
695 956, 10.1038/s41467-018-03027-z, 2018.

696 Riipinen, I., Pierce, J. R., Yli-Juuti, T., Nieminen, T., Hakkinen, S., Ehn, M., Junninen, H.,  
697 Lehtipalo, K., Petaja, T., Slowik, J., Chang, R., Shantz, N. C., Abbatt, J., Leaitch, W. R., Kerminen,  
698 V. M., Worsnop, D. R., Pandis, S. N., Donahue, N. M. and Kulmala, M.: Organic condensation: a  
699 vital link connecting aerosol formation to cloud condensation nuclei (CCN) concentrations,  
700 *Atmos. Chem. Phys.*, 11, 3865-3878, 10.5194/acp-11-3865-2011, 2011.

701 Roldin, P., Eriksson, A. C., Nordin, E. Z., Hermansson, E., Mogensen, D., Rusanen, A., Boy, M.,  
702 Swietlicki, E., Svenningsson, B., Zelenyuk, A. and Pagels, J.: Modelling non-equilibrium  
703 secondary organic aerosol formation and evaporation with the aerosol dynamics, gas- and particle-  
704 phase chemistry kinetic multilayer model ADCHAM, *Atmos. Chem. Phys.*, 14, 7953-7993,  
705 10.5194/acp-14-7953-2014, 2014.

706 Saleh, R., Shihadeh, A. and Khlystov, A.: On transport phenomena and equilibration time scales  
707 in thermodenuders, *Atmos. Meas. Tech.*, 4, 571-581, 10.5194/amt-4-571-2011, 2011.

708 Seinfeld, J. H. and Pandis, S. N.: *Atmospheric chemistry and physics: from air pollution to climate*  
709 *change*, John Wiley & Sons, 2016.

710 Shiraiwa, M., Ammann, M., Koop, T. and Pöschl, U.: Gas uptake and chemical aging of semisolid  
711 organic aerosol particles, *Proc. Natl. Acad. Sci. U.S.A.*, 108, 11003-11008,  
712 10.1073/pnas.1103045108, 2011.

713 Shiraiwa, M., Pfrang, C., Koop, T. and Pöschl, U.: Kinetic multi-layer model of gas-particle  
714 interactions in aerosols and clouds (KM-GAP): linking condensation, evaporation and chemical  
715 reactions of organics, oxidants and water, *Atmos. Chem. Phys.*, 12, 2777-2794, 10.5194/acp-12-  
716 2777-2012, 2012.

717 Shiraiwa, M. and Seinfeld, J. H.: Equilibration timescale of atmospheric secondary organic aerosol  
718 partitioning, *Geophys. Res. Lett.*, 39, L24801, 10.1029/2012GL054008, 2012.

719 Shiraiwa, M., Yee, L. D., Schilling, K. A., Loza, C. L., Craven, J. S., Zuend, A., Ziemann, P. J.  
720 and Seinfeld, J. H.: Size distribution dynamics reveal particle-phase chemistry in organic aerosol  
721 formation, *Proc. Natl. Acad. Sci. U.S.A.*, 110, 11746-11750, 10.1073/pnas.1307501110, 2013a.

722 Shiraiwa, M., Zuend, A., Bertram, A. K. and Seinfeld, J. H.: Gas-particle partitioning of  
723 atmospheric aerosols: interplay of physical state, non-ideal mixing and morphology, *Phys. Chem.*  
724 *Chem. Phys.*, 15, 11441-11453, 10.1039/C3CP51595H, 2013b.

725 Shiraiwa, M., Berkemeier, T., Schilling-Fahnestock, K. A., Seinfeld, J. H. and Pöschl, U.:  
726 Molecular corridors and kinetic regimes in the multiphase chemical evolution of secondary organic  
727 aerosol, *Atmos. Chem. Phys.*, 14, 8323-8341, 10.5194/acp-14-8323-2014, 2014.

728 Shiraiwa, M., Li, Y., Tsimpidi, A. P., Karydis, V. A., Berkemeier, T., Pandis, S. N., Lelieveld, J.,  
729 Koop, T. and Pöschl, U.: Global distribution of particle phase state in atmospheric secondary  
730 organic aerosols, *Nat. Commun.*, 8, 15002, 10.1038/ncomms15002, 2017.

731 Shrivastava, M., Cappa, C. D., Fan, J., Goldstein, A. H., Guenther, A. B., Jimenez, J. L., Kuang,  
732 C., Laskin, A., Martin, S. T., Ng, N. L., Petaja, T., Pierce, J. R., Rasch, P. J., Roldin, P., Seinfeld,  
733 J. H., Shilling, J., Smith, J. N., Thornton, J. A., Volkamer, R., Wang, J., Worsnop, D. R., Zaveri,  
734 R. A., Zelenyuk, A. and Zhang, Q.: Recent advances in understanding secondary organic aerosol:  
735 Implications for global climate forcing, *Rev. Geophys.*, 55, 509-559, 10.1002/2016RG000540,  
736 2017a.

737 Shrivastava, M., Lou, S., Zelenyuk, A., Easter, R. C., Corley, R. A., Thrall, B. D., Rasch, P. J.,  
738 Fast, J. D., Massey Simonich, S. L., Shen, H. and Tao, S.: Global long-range transport and lung  
739 cancer risk from polycyclic aromatic hydrocarbons shielded by coatings of organic aerosol, *Proc.*  
740 *Natl. Acad. Sci. U.S.A.*, 114, 1246-1251, 2017b.

741 Slade, J. H., Shiraiwa, M., Arangio, A., Su, H., Pöschl, U., Wang, J. and Knopf, D. A.: Cloud  
742 droplet activation through oxidation of organic aerosol influenced by temperature and particle  
743 phase state, *Geophys. Res. Lett.*, 44, 1583-1591, 10.1002/2016GL072424, 2017.

744 Song, M., Liu, P., Martin, S. T. and Bertram, A. K.: Liquid-liquid phase separation in particles  
745 containing secondary organic material free of inorganic salts, *Atmos. Chem. Phys.*, 17, 11261-  
746 11271, 10.5194/acp-17-11261-2017, 2017.

747 Tong, H., Arangio, A. M., Lakey, P. S. J., Berkemeier, T., Liu, F., Kampf, C. J., Brune, W. H.,  
748 Pöschl, U. and Shiraiwa, M.: Hydroxyl radicals from secondary organic aerosol decomposition in  
749 water, *Atmos. Chem. Phys.*, 16, 1761-1771, doi:10.5194/acp-16-1761-2016, 2016.

750 Tong, H., Lakey, P. S. J., Arangio, A. M., Socorro, J., Shen, F., Lucas, K., Brune, W. H., Pöschl,  
751 U. and Shiraiwa, M.: Reactive Oxygen Species Formed by Secondary Organic Aerosols in Water  
752 and Surrogate Lung Fluid, *Environ. Sci. Technol.*, 52, 11642-11651, 10.1021/acs.est.8b03695,  
753 2018.

754 Tong, H., Zhang, Y., Filippi, A., Wang, T., Li, C., Liu, F., Leppla, D., Kourtchev, I., Wang, K.,  
755 Keskinen, H.-M., Levula, J. T., Arangio, A. M., Shen, F., Ditas, F., Martin, S. T., Artaxo, P.,  
756 Godoi, R. H. M., Yamamoto, C. I., de Souza, R. A. F., Huang, R.-J., Berkemeier, T., Wang, Y.,  
757 Su, H., Cheng, Y., Pope, F. D., Fu, P., Yao, M., Pöhlker, C., Petäjä, T., Kulmala, M., Andreae, M.  
758 O., Shiraiwa, M., Pöschl, U., Hoffmann, T. and Kalberer, M.: Radical Formation by Fine  
759 Particulate Matter Associated with Highly Oxygenated Molecules, *Environ. Sci. Technol.*, 53,  
760 12506-12518, 10.1021/acs.est.9b05149, 2019.

761 Tröstl, J., Chuang, W. K., Gordon, H., Heinritzi, M., Yan, C., Molteni, U., Ahlm, L., Frege, C.,  
762 Bianchi, F., Wagner, R., Simon, M., Lehtipalo, K., Williamson, C., Craven, J. S., Duplissy, J.,  
763 Adamov, A., Almeida, J., Bernhammer, A.-K., Breitenlechner, M., Brilke, S., Dias, A., Ehrhart,  
764 S., Flagan, R. C., Franchin, A., Fuchs, C., Guida, R., Gysel, M., Hansel, A., Hoyle, C. R., Jokinen,  
765 T., Junninen, H., Kangasluoma, J., Keskinen, H., Kim, J., Krapf, M., Kürten, A., Laaksonen, A.,  
766 Lawler, M., Leiminger, M., Mathot, S., Möhler, O., Nieminen, T., Onnela, A., Petäjä, T., Piel, F.  
767 M., Miettinen, P., Rissanen, M. P., Rondo, L., Sarnela, N., Schobesberger, S., Sengupta, K., Sipilä,  
768 M., Smith, J. N., Steiner, G., Tomè, A., Virtanen, A., Wagner, A. C., Weingartner, E., Wimmer,  
769 D., Winkler, P. M., Ye, P., Carslaw, K. S., Curtius, J., Dommen, J., Kirkby, J., Kulmala, M.,  
770 Riipinen, I., Worsnop, D. R., Donahue, N. M. and Baltensperger, U.: The role of low-volatility  
771 organic compounds in initial particle growth in the atmosphere, *Nature*, 533, 527-531,  
772 10.1038/nature18271, 2016.

773 Trump, E. R. and Donahue, N. M.: Oligomer formation within secondary organic aerosols:  
774 equilibrium and dynamic considerations, *Atmos. Chem. Phys.*, 14, 3691-3701, 10.5194/acp-14-  
775 3691-2014, 2014.

776 Trump, E. R., Riipinen, I. and Donahue, N. M.: Interactions between atmospheric ultrafine  
777 particles and secondary organic aerosol mass: a model study, 2014.

778 Tsigaridis, K., Daskalakis, N., Kanakidou, M., Adams, P. J., Artaxo, P., Bahadur, R., Balkanski,  
779 Y., Bauer, S. E., Bellouin, N., Benedetti, A., Bergman, T., Berntsen, T. K., Beukes, J. P., Bian, H.,  
780 Carslaw, K. S., Chin, M., Curci, G., Diehl, T., Easter, R. C., Ghan, S. J., Gong, S. L., Hodzic, A.,  
781 Hoyle, C. R., Iversen, T., Jathar, S., Jimenez, J. L., Kaiser, J. W., Kirkevåg, A., Koch, D., Kokkola,  
782 H., Lee, Y. H., Lin, G., Liu, X., Luo, G., Ma, X., Mann, G. W., Mihalopoulos, N., Morcrette, J. J.,  
783 Müller, J. F., Myhre, G., Myriokefalitakis, S., Ng, N. L., O'Donnell, D., Penner, J. E., Pozzoli, L.,  
784 Pringle, K. J., Russell, L. M., Schulz, M., Sciare, J., Seland, Ø., Shindell, D. T., Sillman, S., Skeie,  
785 R. B., Spracklen, D., Stavrou, T., Steenrod, S. D., Takemura, T., Tiitta, P., Tilmes, S., Tost, H.,  
786 van Noije, T., van Zyl, P. G., von Salzen, K., Yu, F., Wang, Z., Wang, Z., Zaveri, R. A., Zhang,  
787 H., Zhang, K., Zhang, Q. and Zhang, X.: The AeroCom evaluation and intercomparison of organic  
788 aerosol in global models, *Atmos. Chem. Phys.*, 14, 10845-10895, 10.5194/acp-14-10845-2014,  
789 2014.

790 Vaden, T. D., Imre, D., Beranek, J., Shrivastava, M. and Zelenyuk, A.: Evaporation kinetics and  
791 phase of laboratory and ambient secondary organic aerosol, *Proc. Natl. Acad. Sci. U.S.A.*, 108,  
792 2190-2195, 10.1073/pnas.1013391108, 2011.

793 Vander Wall, A. C., Lakey, P. S. J., Rossich Molina, E., Perraud, V., Wingen, L. M., Xu, J.,  
794 Soulsby, D., Gerber, R. B., Shiraiwa, M. and Finlayson-Pitts, B. J.: Understanding interactions of  
795 organic nitrates with the surface and bulk of organic films: implications for particle growth in the  
796 atmosphere, *Environ. Sci. Processes Impacts*, 20, 1593-1610, 10.1039/C8EM00348C, 2018.

797 Virtanen, A., Joutsensaari, J., Koop, T., Kannosto, J., Yli-Pirilä, P., Leskinen, J., Mäkelä, J. M.,  
798 Holopainen, J. K., Pöschl, U. and Kulmala, M.: An amorphous solid state of biogenic secondary  
799 organic aerosol particles, *Nature*, 467, 824-827, 2010.

800 Von Domaros, M., Lakey, P. S. J., Shiraiwa, M. and Tobias, D. J.: Multiscale Modeling of Human  
801 Skin Oil-Induced Indoor Air Chemistry: Combining Kinetic Models and Molecular Dynamics, *J.*  
802 *Phys. Chem. B*, 124, 3836-3843, 10.1021/acs.jpcc.0c02818, 2020.

803 Wei, J., Fang, T., Wong, C., Lakey, P. S. J., Nizkorodov, S. A. and Shiraiwa, M.: Superoxide  
804 Formation from Aqueous Reactions of Biogenic Secondary Organic Aerosols, *Environ. Sci.*  
805 *Technol.*, es-2020-07789e, 2020.

806 Winkler, P. M., Vrtala, A., Wagner, P. E., Kulmala, M., Lehtinen, K. E. J. and Vesala, T.: Mass  
807 and thermal accommodation during gas-liquid condensation of water, *Phys. Rev. Lett.*, 93, 075701,  
808 10.1103/PhysRevLett.93.075701, 2004.

809 Winkler, P. M., Vrtala, A., Rudolf, R., Wagner, P. E., Riipinen, I., Vesala, T., Lehtinen, K. E. J.,  
810 Viisanen, Y. and Kulmala, M.: Condensation of water vapor: Experimental determination of mass  
811 and thermal accommodation coefficients, *J. Geophys. Res.-Atmos.*, 111, D19202,  
812 10.1029/2006jd007194, 2006.

813 Worsnop, D. R., Morris, J. W., Shi, Q., Davidovits, P. and Kolb, C. E.: A chemical kinetic model  
814 for reactive transformations of aerosol particles, *Geophys. Res. Lett.*, 29, 57,  
815 10.1029/2002gl015542, 2002.

816 Ye, Q., Robinson, E. S., Ding, X., Ye, P., Sullivan, R. C. and Donahue, N. M.: Mixing of secondary  
817 organic aerosols versus relative humidity, *Proc. Natl. Acad. Sci. U.S.A.*, 113, 12649-12654, 2016.

818 Ye, Q., Upshur, M. A., Robinson, E. S., Geiger, F. M., Sullivan, R. C., Thomson, R. J. and  
819 Donahue, N. M.: Following Particle-Particle Mixing in Atmospheric Secondary Organic Aerosols  
820 by Using Isotopically Labeled Terpenes, *Chem*, 4, 318-333, 10.1016/j.chempr.2017.12.008, 2018.

821 Yli-Juuti, T., Pajunoja, A., Tikkanen, O.-P., Buchholz, A., Faiola, C., Väisänen, O., Hao, L., Kari,  
822 E., Peräkylä, O., Garmash, O., Shiraiwa, M., Ehn, M., Lehtinen, K. and Virtanen, A.: Factors  
823 controlling the evaporation of secondary organic aerosol from  $\alpha$ -pinene ozonolysis, *Geophys. Res.*  
824 *Lett.*, 44, 2562-2570, 10.1002/2016GL072364, 2017.

825 You, Y., Smith, M. L., Song, M., Martin, S. T. and Bertram, A. K.: Liquid-liquid phase separation  
826 in atmospherically relevant particles consisting of organic species and inorganic salts, *Int. Rev.*  
827 *Phys. Chem.*, 33, 43-77, 10.1080/0144235x.2014.890786, 2014.

828 Zaveri, R. A., Easter, R. C., Shilling, J. E. and Seinfeld, J. H.: Modeling kinetic partitioning of  
829 secondary organic aerosol and size distribution dynamics: representing effects of volatility, phase  
830 state, and particle-phase reaction, *Atmos. Chem. Phys.*, 14, 5153-5181, 10.5194/acp-14-5153-  
831 2014, 2014.

832 Zaveri, R. A., Shilling, J. E., Zelenyuk, A., Liu, J., Bell, D. M., D'Ambro, E. L., Gaston, C. J.,  
833 Thornton, J. A., Laskin, A., Lin, P., Wilson, J., Easter, R. C., Wang, J., Bertram, A. K., Martin, S.  
834 T., Seinfeld, J. H. and Worsnop, D. R.: Growth Kinetics and Size Distribution Dynamics of  
835 Viscous Secondary Organic Aerosol, *Environ. Sci. Technol.*, 52, 1191-1199,  
836 10.1021/acs.est.7b04623, 2018.

837 Zaveri, R. A., Shilling, J. E., Zelenyuk, A., Zawadowicz, M. A., Suski, K., China, S., Bell, D. M.,  
838 Veghte, D. and Laskin, A.: Particle-Phase Diffusion Modulates Partitioning of Semivolatile  
839 Organic Compounds to Aged Secondary Organic Aerosol, *Environ. Sci. Technol.*, 54, 2595-2605,  
840 10.1021/acs.est.9b05514, 2020.

841 Zhang, Y., Chen, Y., Lambe, A. T., Olson, N. E., Lei, Z., Craig, R. L., Zhang, Z., Gold, A., Onasch,  
842 T. B., Jayne, J. T., Worsnop, D. R., Gaston, C. J., Thornton, J. A., Vizuete, W., Ault, A. P. and  
843 Surratt, J. D.: Effect of the Aerosol-Phase State on Secondary Organic Aerosol Formation from  
844 the Reactive Uptake of Isoprene-Derived Epoxydiols (IEPOX), *Environ. Sci. Technol. Lett.*,  
845 10.1021/acs.estlett.8b00044, 2018.

846 Zhou, S., Shiraiwa, M., McWhinney, R., Pöschl, U. and Abbatt, J. P. D.: Kinetic limitations in  
847 gas-particle reactions arising from slow diffusion in secondary organic aerosol, *Faraday Discuss.*,  
848 165, 391-406, 10.1039/C3FD00030C, 2013.

849 Zhou, S., Hwang, B. C. H., Lakey, P. S. J., Zuend, A., Abbatt, J. P. D. and Shiraiwa, M.:  
850 Multiphase reactivity of polycyclic aromatic hydrocarbons is driven by phase separation and



851 diffusion limitations, Proc. Natl. Acad. Sci. U.S.A., 116, 11658-11663, 10.1073/pnas.1902517116,  
852 2019.

853 Ziemann, P. J. and Atkinson, R.: Kinetics, products, and mechanisms of secondary organic aerosol  
854 formation, Chem. Soc. Rev., 41, 6582-6605, 2012.

855 Zuend, A. and Seinfeld, J. H.: Modeling the gas-particle partitioning of secondary organic aerosol:  
856 the importance of liquid-liquid phase separation, Atmos. Chem. Phys., 12, 3857-3882,  
857 10.5194/acp-12-3857-2012, 2012.

858

859